

Multiloop flow equations for single-boson exchange fRG

Elias Walter¹, Marcel Gievers^{1,2}, Anxiang Ge¹, Jan von Delft¹, and Fabian B. Kugler³

¹ Arnold Sommerfeld Center for Theoretical Physics, Center for NanoScience, and Munich Center for Quantum Science and Technology, Ludwig-Maximilians-Universität München, 80333 Munich, Germany

² Max Planck Institute of Quantum Optics, Hans-Kopfermann-Straße 1, 85748 Garching, Germany

³ Department of Physics and Astronomy, Rutgers University, Piscataway, New Jersey 08854, USA

January 14, 2022

Abstract The recently introduced single-boson exchange (SBE) decomposition of the four-point vertex of interacting fermionic many-body theories constitutes a conceptually and computationally appealing parametrization of the vertex. It relies on the notion of reducibility of vertex diagrams with respect to the bare interaction U , instead of a classification based on two-particle reducibility within the widely-used parquet decomposition. Here, we construct a general form of the SBE decomposition following from the parquet equations, and derive multiloop functional renormalization group (mfRG) flow equations for the constituents of this SBE decomposition. Along the way, we also derive mfRG flow equations for the often-used decomposition of the vertex in terms of asymptotic classes of the two-particle reducible vertices. We show that the two decompositions are closely related, with mfRG flow equations very similar in structure.

PACS. XX.XX.XX No PACS code given

1 Introduction

The understanding of strongly correlated many-body systems like the two-dimensional Hubbard model remains an important challenge of contemporary condensed-matter physics [1]. For this, it is desirable to gain profound understanding of two-body interactions which are described by the full four-point vertex Γ .

A powerful technique for calculating the four-point vertex Γ is the functional renormalization group (fRG) [2, 3]. There, a scale parameter Λ is introduced into the bare Green's function $G_0 \rightarrow G_0^\Lambda$ in such a way that for an initial value $\Lambda \rightarrow \Lambda_i$ the theory (specifically, the calculation of the self-energy Σ^Λ and the four-point vertex Γ^Λ) becomes solvable, and after successively integrating out higher-energy modes $\Lambda \rightarrow \Lambda_f$, the fully correlated objects Σ and Γ are obtained.

Traditionally, fRG is formulated through an infinite hierarchy of exact flow equations for n -point vertex functions. However, since already the six-point vertex is numerically intractable, truncations are needed. A frequently-used strategy employs a one-loop (1ℓ) truncation of the exact hierarchy of flow equations by completely neglecting six-point and higher vertices. This can be justified, e.g., from a perturbative [2] or leading-log [4] perspective. Another truncation scheme is given by the multiloop fRG approach, mfRG, which includes all contributions of the six-point vertex to the flow of the four-point vertex and self-energy that can be computed with numerical costs proportional to the 1ℓ flow [5–7]. In doing so, it sums up

all parquet diagrams, formally reconstructing the parquet approximation (PA) [8, 9] if loop convergence is achieved. Converged multiloop results thus inherit all the properties of the PA. These include self-consistency at the one- and two-particle level (in that the PA is a solution of the self-consistent parquet equations [9]); the validity of one-particle conservation laws (but not of two-particle ones); and the independence of the final results on the choice of regulator (since the parquet equations and PA do not involve specifying any regulator).

A full treatment of the frequency and momentum dependence of the four-point vertex generally requires tremendous numerical resources. Thus, it is important to parametrize these dependencies in an efficient way, to reduce computational effort without losing information on important physical properties. One such scheme expresses the vertex as a sum of diagrammatic classes distinguished by their asymptotic frequency behavior [10, 11]. This reduces numerical costs: Asymptotic classes which remain nonzero when one or two frequency arguments are sent to infinity do not depend on these arguments, while the class depending on all three frequency arguments decays in each direction. A related strategy is to decompose the vertex into fermion bilinears that interact via exchange bosons [12, 13]. This idea also underlies the single-boson exchange (SBE) formalism [14–18], where the vertex is decomposed regarding its reducibility in the bare interaction U . Physically, this corresponds to parametrizing the vertex in terms of bosonic fluctuations and their (Yukawa) couplings to fermions through Hedin

are two-particle reducible in channel r , i.e., they can be split into two parts by cutting two antiparallel (a), parallel (p), or transverse antiparallel (t) propagator lines, respectively. The diagrams in R do not fall apart by cutting two propagator lines and are thus fully two-particle irreducible. Importantly, this classification is exact and unambiguous [11, 28]. In the literature, the diagrammatic channels are also known as crossed particle-hole ($\overline{\text{ph}} \leftrightarrow a$), particle-particle ($\text{pp} \leftrightarrow p$), and particle-hole ($\text{ph} \leftrightarrow t$) channel.

Since the four classes in the parquet decomposition are disjoint, one can decompose Γ w.r.t. its two-particle reducibility in one of the channels r , $\Gamma = I_r + \gamma_r$. Here, I_r comprises the sum of all diagrams irreducible in channel r and fulfills $I_r = R + \gamma_{\bar{r}}$ with $\gamma_{\bar{r}} = \sum_{r' \neq r} \gamma_{r'}$. The Bethe–Salpeter equations (BSE) relate the irreducible diagrams to the reducible ones and can be summarized by

$$\gamma_r = I_r \circ \Pi_r \circ \Gamma = \Gamma \circ \Pi_r \circ I_r. \quad (4)$$

Here, the Π_r bubble, defined as

$$\Pi_{a;34|3'4'} = G_{3|3'} G_{4|4'}, \quad (5a)$$

$$\Pi_{p;34|3'4'} = \frac{1}{2} G_{3|3'} G_{4|4'}, \quad (5b)$$

$$\Pi_{t;43|3'4'} = -G_{3|3'} G_{4|4'}, \quad (5c)$$

represents the corresponding propagator pair in channel r , see Fig. 1. (Note that $\Pi_{a;34|3'4'} = -\Pi_{t;43|3'4'}$ is consistent with crossing symmetry.) The connector symbol \circ denotes summation over internal frequencies and quantum numbers (5, 6 in Eq. (6) below) and its definition depends on the channel $r \in \{a, p, t\}$: When connecting Π_r (or other four-leg objects labeled by r) to some vertex, it gives

$$a: [A \circ B]_{12|34} = A_{16|54} B_{52|36}, \quad (6a)$$

$$p: [A \circ B]_{12|34} = A_{12|56} B_{56|34}, \quad (6b)$$

$$t: [A \circ B]_{12|34} = A_{62|54} B_{15|36}. \quad (6c)$$

By combining $\Gamma = I_r + \gamma_r$ with the BSE (4), one can eliminate γ_r to get the extended BSE [7] needed later:

$$\mathbb{1}_r + \Pi_r \circ \Gamma = (\mathbb{1}_r - \Pi_r \circ I_r)^{-1}, \quad (7a)$$

$$\mathbb{1}_r + \Gamma \circ \Pi_r = (\mathbb{1}_r - I_r \circ \Pi_r)^{-1}. \quad (7b)$$

Here, the channel-specific unit vertices $\mathbb{1}_r$, defined by the requirement $\Gamma = \mathbb{1}_r \circ \Gamma = \Gamma \circ \mathbb{1}_r$, are given by

$$\mathbb{1}_{a;12|34} = \delta_{13} \delta_{24} = \mathbb{1}_{p;12|34}, \quad \mathbb{1}_{t;12|34} = \delta_{14} \delta_{23}. \quad (8)$$

The combination of the Dyson equation $G = G_0(1 + \Sigma G)$, the Schwinger–Dyson equation, the parquet decomposition (3), the three BSE (4), and the definitions $I_r = \Gamma - \gamma_r$ constitutes the self-consistent *parquet equations*. The only truly independent object is the fully irreducible vertex R . If R is specified, everything else can be computed self-consistently via the parquet equations. However, R itself is the most complicated object: R diagrams contain several nested integrals/sums over internal arguments, whereas the integrals in reducible diagrams

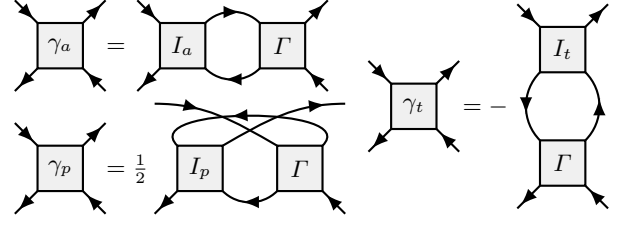


Figure 1. Bethe–Salpeter equations in the antiparallel (a), parallel (p) and transverse (t) channels.

partially factorize. This makes R diagrams beyond the bare vertex hardly tractable numerically. A common simplification, the parquet approximation (PA), replaces R by U ; the resulting closed set of equations defines an infinite set of diagrams, the so-called *parquet diagrams*. In this work, however, the PA is not used.

2.2 mfRG equations

The mfRG flow equations can be derived from the parquet equations by introducing a regulator Λ into the bare propagator G_0 , thus making all objects in the parquet equations Λ -dependent [7]. Here, the fully irreducible vertex R is treated as an input and is thus assumed to be Λ -independent, $R^\Lambda \approx R$. Taking the derivative of the Schwinger–Dyson equation and the BSE w.r.t. Λ then yields flow equations for Σ and Γ .

When computing $\dot{\gamma}_r = \partial_\Lambda \gamma_r$ via the BSE, one obtains terms including $\dot{I}_r = \sum_{r' \neq r} \dot{\gamma}_{r'}$. Thus, one has to iteratively insert the flow equation for γ_r into the equations of the other channels $r' \neq r$, yielding an infinite set of contributions of increasing “loop order”:

$$\dot{\Gamma} = \dot{\gamma}_a + \dot{\gamma}_p + \dot{\gamma}_t, \quad \dot{\gamma}_r = \sum_{\ell=1}^{\infty} \dot{\gamma}_r^{(\ell)}. \quad (10)$$

The individual ℓ -loop contributions read [5, 7]

$$\dot{\gamma}_r^{(1)} = \Gamma \circ \dot{\Pi}_r \circ \Gamma, \quad (11a)$$

$$\dot{\gamma}_r^{(2)} = \dot{\gamma}_{\bar{r}}^{(1)} \circ \Pi_r \circ \Gamma + \Gamma \circ \Pi_r \circ \dot{\gamma}_{\bar{r}}^{(1)} \quad (11b)$$

$$\begin{aligned} \dot{\gamma}_r^{(\ell+2)} &= \dot{\gamma}_{\bar{r}}^{(\ell+1)} \circ \Pi_r \circ \Gamma + \Gamma \circ \Pi_r \circ \dot{\gamma}_{\bar{r}}^{(\ell)} \circ \Pi_r \circ \Gamma \\ &\quad + \Gamma \circ \Pi_r \circ \dot{\gamma}_{\bar{r}}^{(\ell+1)}. \end{aligned} \quad (11c)$$

where $\dot{\gamma}_{\bar{r}}^{(\ell)} = \sum_{r' \neq r} \dot{\gamma}_{r'}^{(\ell)}$ and Eq. (11c) applies for $\ell+2 \geq 3$. Furthermore, $\dot{\Pi}_r \sim G\dot{G} + \dot{G}G$, where

$$\dot{G} = S + G\dot{\Sigma}G, \quad (12)$$

with the single-scale propagator $S = \dot{G}|_{\Sigma=\text{const}}$. Figure 2 illustrates Eq. (11) diagrammatically in the a channel.

Note that the mfRG flow equations for the self-energy are given in Ref. [7]. We do not need them in this paper, since our focus is on vertex decompositions. Generally, they should of course be implemented, too.

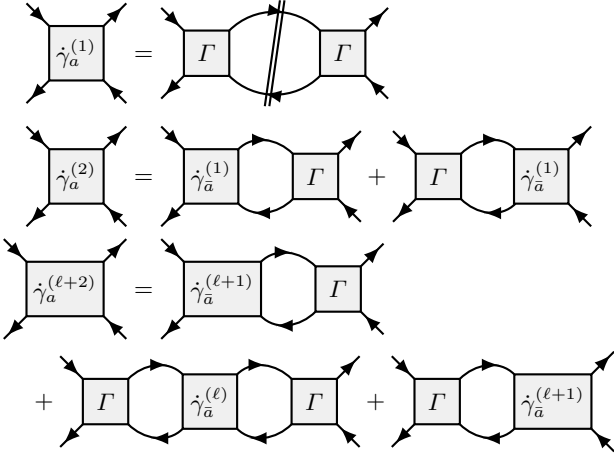


Figure 2. Diagrammatic depiction of the mfRG flow equations (11) in the a channel. The double-dashed bubble \tilde{H}_a represents a sum of two terms, $G\dot{G} + \dot{G}G$, where double-dashed propagators \dot{G} are fully differentiated ones [cf. Eq. (12)].

The 1ℓ contribution (11a) of the vertex flow, with the fully-differentiated \dot{G} replaced by the single-scale propagator S in \tilde{H}_r is equivalent to the usual 1ℓ flow equation. Using \dot{G} instead of S , as done in Eq. (11a), corresponds to the so-called Katanin substitution [29]: it contains the feedback of the differentiated self-energy into the vertex flow and already goes beyond the standard 1ℓ approximation. By adding higher-loop contributions until convergence is reached, one effectively solves the self-consistent parquet equations through an fRG flow. On the one hand, this ensures two-particle self-consistency and related properties mentioned in the introduction. On the other hand, it also provides a way of reaching a solution of the parquet equations by simply integrating differential equations. This may be numerically favorable compared to an iteration of the self-consistent equations. Particularly, when computing diagrammatic extensions of DMFT via DMF²RG, one then needs only the *full* DMFT vertex as an input, and not the r -(ir)reducible ones entering the parquet equations. This is helpful in the Matsubara formalism, where the r -(ir)reducible vertices sometimes exhibit divergences [30–34], and even more so when aiming for real-frequency approaches [35, 36].

3 Asymptotic classes

The four-point vertex Γ is a highly complicated object and must be parametrized efficiently. In this section, we summarize the vertex decomposition into asymptotic classes. The alternative SBE decomposition is discussed in Sec. 4.

We henceforth focus on the frequency dependence of the full vertex. We thus switch from the compact notation $\Gamma_{1'2'|12}$ to the more elaborate $\Gamma_{1'2'|12}(\nu'_1\nu'_2|\nu_1\nu_2)$, with frequency arguments written in brackets, and the subscripts now referring to non-frequency quantum numbers (position or momentum, spin, etc.). As mentioned earlier, we

assume the bare vertex U to have the form

$$U_{1'2'|12}(\nu'_1\nu'_2|\nu_1\nu_2) = \delta_{\nu'_1+\nu'_2, \nu_1+\nu_2} U_{1'2'|12}, \quad (13)$$

with $U_{1'2'|12}$ independent of frequency. If U is momentum-conserving without further momentum dependence, our treatment of frequency sums below may be extended to include momentum sums. To keep the discussion general, we refrain from elaborating this in detail. Note that, e.g., in the repulsive Hubbard model, our sign convention in Eq. (1) is such that $U^{\sigma\bar{\sigma}|\sigma\bar{\sigma}} = -U^{\bar{\sigma}\sigma|\sigma\bar{\sigma}} < 0$ (where, as usual, $\sigma \in \{\uparrow, \downarrow\}$, $\bar{\uparrow} = \downarrow$, $\bar{\downarrow} = \uparrow$).

3.1 Frequency parametrization

The parquet decomposition (3) of the vertex into different diagrammatic channels has direct consequences on the frequency asymptotics [11], as we outline in the following. Due to frequency conservation, three frequencies are sufficient to parametrize the vertex. For each channel r , we express the four fermionic frequencies $\nu'_1, \nu'_2, \nu_1, \nu_2$ at the vertex legs through a choice of three frequencies, a bosonic transfer frequency, ω_r , and two fermionic frequencies, ν_r and ν'_r . These are chosen differently for each channel to make the asymptotic behavior apparent. As shown in Fig. 3, we choose symmetric parametrizations, with $\pm \frac{\omega_r}{2}$ terms on all vertex legs. Thereby, crossing symmetries ensure that prominent vertex peaks are centered around $\omega_r = 0$, which is convenient for numerical work. However, other conventions are of course possible, too. (In the Matsubara formalism, the bosonic Matsubara frequency closest to $\pm \frac{\omega_r}{2}$ is chosen for the shift.)

Though the frequencies ω_r, ν_r, ν'_r are tailored to a specific channel r , one may also use them to define the r parametrization of the full vertex,

$$\Gamma_{1'2'|1,2}(\nu'_1\nu'_2|\nu_1\nu_2) = \delta_{\nu'_1+\nu'_2, \nu_1+\nu_2} \Gamma_{1'2'|1,2}(\omega_r, \nu_r, \nu'_r), \quad (14)$$

Likewise, $R, \gamma_a, \gamma_p, \gamma_t$ can each be expressed as a δ symbol times a function of the *same* set of variables, $(\omega_r, \nu_r, \nu'_r)$. Then, bubbles of the type $\Gamma \circ \Pi_r \circ \tilde{\Gamma}$ can be written as

$$\begin{aligned} & (\Gamma \circ \Pi_r \circ \tilde{\Gamma})(\omega_r, \nu_r, \nu'_r) \\ &= \sum_{\nu''_r} \Gamma(\omega_r, \nu_r, \nu''_r) \bullet \Pi_r(\omega_r, \nu''_r) \bullet \tilde{\Gamma}(\omega_r, \nu''_r, \nu'_r), \end{aligned} \quad (15)$$

with $\Pi_r(\omega_r, \nu''_r)$ given by

$$\Pi_{a;34|3'4'}(\omega_a, \nu''_a) = G_{3|3'}(\nu''_a - \frac{\omega_a}{2}) G_{4|4'}(\nu''_a + \frac{\omega_a}{2}), \quad (16a)$$

$$\Pi_{p;34|3'4'}(\omega_p, \nu''_p) = \frac{1}{2} G_{3|3'}(\frac{\omega_p}{2} + \nu''_p) G_{4|4'}(\frac{\omega_p}{2} - \nu''_p), \quad (16b)$$

$$\Pi_{t;43|3'4'}(\omega_t, \nu''_t) = -G_{3|3'}(\nu''_t - \frac{\omega_t}{2}) G_{4|4'}(\nu''_t + \frac{\omega_t}{2}). \quad (16c)$$

The connector \bullet in Eq. (15) denotes an internal summation analogous to \circ , except that only non-frequency quantum numbers (position, spin, etc.) are summed over, since the frequency sum has been displayed explicitly. Corresponding unit vertices for non-frequency quantum numbers, $\mathbf{1}_r$, are defined by $\Gamma = \mathbf{1}_r \bullet \Gamma = \Gamma \bullet \mathbf{1}_r$. The distinction between $\circ, \mathbb{1}$ and $\bullet, \mathbf{1}$, indicating whether connectors and

$$\Gamma(\nu'_1\nu'_2|\nu_1\nu_2) = \left[R(\omega_r, \nu_r, \nu'_r) + \gamma_a(\omega_a, \nu_a, \nu'_a) + \gamma_p(\omega_p, \nu_p, \nu'_p) + \gamma_t(\omega_t, \nu_t, \nu'_t) \right] \delta_{\nu'_1+\nu'_2, \nu_1+\nu_2}$$

Figure 3. Definition of the three natural frequency parametrizations of the four-point vertex. The vertex is nonzero only if the four fermionic frequencies satisfy $\nu'_1 + \nu'_2 = \nu_1 + \nu_2$. In that case, they can be expressed in three different ways through one bosonic transfer frequency, ω_r , and two fermionic frequencies, ν_r, ν'_r . Each of these choices is “natural” for the corresponding channel r , and convenient for describing the high-frequency asymptotics of γ_r . Of course, each term can be expressed through the frequencies $(\omega_r, \nu_r, \nu'_r)$ of any of the three channels, as indicated here for R .

unit vertices include summations and δ symbols for frequency variables or not, will be needed for the SBE decomposition of Sec. 4. (For a bare vertex with momentum conservation and no further momentum dependence, one could include a momentum sum, $\sum_{k''}$, in Eq. (15), and exclude momentum indices from the \bullet summation and $\mathbf{1}_r$.)

3.2 Definition of asymptotic classes

The decomposition of each two-particle reducible vertex γ_r into asymptotic classes was introduced in [11] to conveniently express the high-frequency asymptotics of the vertices through simpler objects with fewer frequency arguments. We make the ansatz

$$\begin{aligned} \gamma_r(\omega_r, \nu_r, \nu'_r) & \\ &= \mathcal{K}_1^r(\omega_r) + \mathcal{K}_2^r(\omega_r, \nu_r) + \mathcal{K}_{2'}^r(\omega_r, \nu'_r) + \mathcal{K}_3^r(\omega_r, \nu_r, \nu'_r). \end{aligned} \quad (17)$$

(For a diagrammatic depiction, see App. A, Fig. 10.) Here, \mathcal{K}_1^r contains all diagrams having both ν_r legs connected to the same bare vertex and both ν'_r legs connected to another bare vertex. These diagrams are thus independent of ν_r, ν'_r and stay finite in the limit $|\nu_r| \rightarrow \infty, |\nu'_r| \rightarrow \infty$,

$$\lim_{|\nu_r| \rightarrow \infty} \lim_{|\nu'_r| \rightarrow \infty} \gamma_r(\omega_r, \nu_r, \nu'_r) = \mathcal{K}_1^r(\omega_r). \quad (18a)$$

\mathcal{K}_2^r (or $\mathcal{K}_{2'}^r$) analogously contains the part of the vertex having both ν'_r (or ν_r) legs connected to the same bare vertex while the two ν_r (or ν'_r) legs are connected to different bare vertices. Hence, it is finite for $|\nu'_r| \rightarrow \infty$ (or $|\nu_r| \rightarrow \infty$) but vanishes for $|\nu_r| \rightarrow \infty$ (or $|\nu'_r| \rightarrow \infty$):

$$\begin{aligned} \lim_{|\nu'_r| \rightarrow \infty} \gamma_r(\omega_r, \nu_r, \nu'_r) &= \mathcal{K}_1^r(\omega_r) + \mathcal{K}_2^r(\omega_r, \nu_r), \\ \lim_{|\nu_r| \rightarrow \infty} \gamma_r(\omega_r, \nu_r, \nu'_r) &= \mathcal{K}_1^r(\omega_r) + \mathcal{K}_{2'}^r(\omega_r, \nu'_r). \end{aligned} \quad (18b)$$

\mathcal{K}_3^r exclusively contains diagrams having both ν_r legs connected to different bare vertices, and likewise for both ν'_r legs. Such diagrams depend on all three frequencies and thus decay if any of them is sent to infinity. When taking

the above limits for bubbles involving channels r' different from r , we obtain zero,

$$\lim_{|\nu_r| \rightarrow \infty} \gamma_{r' \neq r} = \lim_{|\nu'_r| \rightarrow \infty} \gamma_{r' \neq r} = 0, \quad (18c)$$

since each $\Pi_{r'}$ in $\gamma_{r'}$ has a denominator containing $\omega_{r' \neq r}$, which is a linear combination of ω_r, ν_r and ν'_r .

Since R explicitly depends on all frequencies, it decays to the bare vertex U at high frequencies, and the asymptotic classes can be obtained by taking limits of the full vertex. Explicitly, \mathcal{K}_1^r can be obtained from

$$\lim_{|\nu_r| \rightarrow \infty} \lim_{|\nu'_r| \rightarrow \infty} \Gamma(\omega_r, \nu_r, \nu'_r) = U + \mathcal{K}_1^r(\omega_r), \quad (19a)$$

taking the double limit in such a way that $\nu_r \pm \nu'_r$ is not constant, to ensure that all bosonic frequencies $|\omega_{r' \neq r}|$ go to ∞ [11]. Similarly, $\mathcal{K}_2^r, \mathcal{K}_{2'}^r$ can be obtained from objects $\Gamma_2^r, \Gamma_{2'}^r$ defined via the limits

$$\Gamma_2^r(\omega_r, \nu_r) = \lim_{|\nu'_r| \rightarrow \infty} \Gamma(\omega_r, \nu_r, \nu'_r) = U + \mathcal{K}_1^r + \mathcal{K}_2^r, \quad (19b)$$

$$\Gamma_{2'}^r(\omega_r, \nu'_r) = \lim_{|\nu_r| \rightarrow \infty} \Gamma(\omega_r, \nu_r, \nu'_r) = U + \mathcal{K}_1^r + \mathcal{K}_{2'}^r. \quad (19c)$$

For each of the latter two limits, we denote the complementary part of the vertex (vanishing in said limit) by

$$\bar{\Gamma}_2^r(\omega_r, \nu_r, \nu'_r) = \Gamma - \Gamma_2^r = \mathcal{K}_{2'}^r + \mathcal{K}_3^r + \gamma_{\bar{r}} + R - U, \quad (19d)$$

$$\bar{\Gamma}_{2'}^r(\omega_r, \nu_r, \nu'_r) = \Gamma - \Gamma_{2'}^r = \mathcal{K}_2^r + \mathcal{K}_3^r + \gamma_{\bar{r}} + R - U. \quad (19e)$$

By taking suitable limits in the BSE (4), the asymptotic classes can be expressed through the full vertex Γ and the bare interaction U [11]:

$$\mathcal{K}_1^r(\omega_r) = U \circ (\Pi_r + \Pi_r \circ \Gamma \circ \Pi_r) \circ U, \quad (20a)$$

$$\mathcal{K}_2^r(\omega_r, \nu_r) = \Gamma \circ \Pi_r \circ U - \mathcal{K}_1^r, \quad (20b)$$

$$\mathcal{K}_{2'}^r(\omega_r, \nu'_r) = U \circ \Pi_r \circ \Gamma - \mathcal{K}_1^r. \quad (20c)$$

Using Eq. (15), we can also express \mathcal{K}_1^r as

$$\mathcal{K}_1^r(\omega_r) = U \bullet \chi_r(\omega_r) \bullet U, \quad (21a)$$

$$\chi_r(\omega_r) = \sum_{\nu''} \Pi_r(\omega_r, \nu''_r) \quad (21b)$$

$$+ \sum_{\nu_r, \nu'_r} \Pi_r(\omega_r, \nu_r) \bullet \Gamma(\omega_r, \nu_r, \nu'_r) \bullet \Pi_r(\omega_r, \nu'_r),$$

where χ_r represents a susceptibility. (The bare vertices were pulled out in front of the frequency sums, exploiting their frequency independence.) The relation of χ_r to physical susceptibilities for a local bare interaction U is discussed in App. B.

3.3 mfRG equations for asymptotic classes

When the vertex is represented through its asymptotic classes, it is convenient to compute the latter directly during the flow, without numerically sending certain frequencies to infinity. This facilitates systematically adding or neglecting higher asymptotic classes. Therefore, we now derive explicit mfRG flow equations for the asymptotic classes, starting from the general multiloop flow equations (11). (For a diagrammatic derivation, see Refs. [37, 38].)

The decomposition (17) of γ_r into asymptotic classes holds analogously at each loop order,

$$\dot{\gamma}_r^{(\ell)} = \dot{\mathcal{K}}_1^{r(\ell)} + \dot{\mathcal{K}}_2^{r(\ell)} + \dot{\mathcal{K}}_{2'}^{r(\ell)} + \dot{\mathcal{K}}_3^{r(\ell)}. \quad (22)$$

These constituents can be obtained from Eqs. (11) for $\dot{\gamma}_r^{(\ell)}$ by taking suitable limits of the fermionic frequencies ν_r, ν_r' , as specified in Eqs. (18). For example, consider a bubble of type $\Gamma \circ \dot{\Pi}_r \circ \tilde{\Gamma}$, in the r representation of Eq. (15). In the limit $|\nu_r| \rightarrow \infty$, the first vertex reduces to $\Gamma_{2'}^r$ [Eq. (19c)], while for $|\nu_r'| \rightarrow \infty$, the second vertex reduces to $\tilde{\Gamma}_2^r$ [Eq. (19b)]. By Eq. (15), we thus obtain

$$\lim_{|\nu_r| \rightarrow \infty} \Gamma \circ \dot{\Pi}_r \circ \tilde{\Gamma} = \Gamma_{2'}^r \circ \dot{\Pi}_r \circ \tilde{\Gamma}, \quad (23a)$$

$$\lim_{|\nu_r'| \rightarrow \infty} \Gamma \circ \dot{\Pi}_r \circ \tilde{\Gamma} = \Gamma \circ \dot{\Pi}_r \circ \tilde{\Gamma}_2^r. \quad (23b)$$

By contrast, when taking these limits for bubbles involving channels r' different from r , we obtain zero,

$$\lim_{|\nu_r| \rightarrow \infty} \Gamma \circ \dot{\Pi}_{r' \neq r} \circ \tilde{\Gamma} = 0, \quad \lim_{|\nu_r'| \rightarrow \infty} \Gamma \circ \dot{\Pi}_{r' \neq r} \circ \tilde{\Gamma} = 0, \quad (23c)$$

by similar reasoning as that leading to Eq. (18c). In this manner, the 1ℓ flow equation (11a) for $\dot{\gamma}_r^{(1)}$ readily yields

$$\begin{aligned} \dot{\mathcal{K}}_1^{r(1)} &= \Gamma_{2'}^r \circ \dot{\Pi}_r \circ \Gamma_2^r, \\ \dot{\mathcal{K}}_2^{r(1)} &= \tilde{\Gamma}_2^r \circ \dot{\Pi}_r \circ \Gamma_2^r, \\ \dot{\mathcal{K}}_{2'}^{r(1)} &= \Gamma_{2'}^r \circ \dot{\Pi}_r \circ \tilde{\Gamma}_2^r, \\ \dot{\mathcal{K}}_3^{r(1)} &= \tilde{\Gamma}_2^r \circ \dot{\Pi}_r \circ \tilde{\Gamma}_2^r. \end{aligned} \quad (24a)$$

Similarly, the two-loop contribution $\dot{\gamma}_r^{(2)}$, Eq. (11b), yields

$$\begin{aligned} \dot{\mathcal{K}}_1^{r(2)} &= 0, \\ \dot{\mathcal{K}}_2^{r(2)} &= \dot{\gamma}_{\tilde{r}}^{(1)} \circ \Pi_r \circ \Gamma_2^r, \\ \dot{\mathcal{K}}_{2'}^{r(2)} &= \Gamma_{2'}^r \circ \Pi_r \circ \dot{\gamma}_{\tilde{r}}^{(1)}, \\ \dot{\mathcal{K}}_3^{r(2)} &= \dot{\gamma}_{\tilde{r}}^{(1)} \circ \Pi_r \circ \tilde{\Gamma}_2^r + \tilde{\Gamma}_2^r \circ \Pi_r \circ \dot{\gamma}_{\tilde{r}}^{(1)}. \end{aligned} \quad (24b)$$

Due to Eq. (18c), $\dot{\mathcal{K}}_1^{r(2)}$ vanishes and $\dot{\mathcal{K}}_2^{r(2)}$ or $\dot{\mathcal{K}}_{2'}^{r(2)}$ contain no terms with $\dot{\gamma}_{\tilde{r}}^{(1)}$ on their right or left sides, respectively. Finally, Eq. (11c) for $\dot{\gamma}_r^{(\ell+2)}$, with $\ell \geq 1$, yields

$$\begin{aligned} \dot{\mathcal{K}}_1^{r(\ell+2)} &= \Gamma_{2'}^r \circ \Pi_r \circ \dot{\gamma}_{\tilde{r}}^{(\ell)} \circ \Pi_r \circ \Gamma_2^r, \\ \dot{\mathcal{K}}_2^{r(\ell+2)} &= \dot{\gamma}_{\tilde{r}}^{(\ell+1)} \circ \Pi_r \circ \Gamma_2^r + \tilde{\Gamma}_2^r \circ \Pi_r \circ \dot{\gamma}_{\tilde{r}}^{(\ell)} \circ \Pi_r \circ \Gamma_2^r, \\ \dot{\mathcal{K}}_{2'}^{r(\ell+2)} &= \Gamma_{2'}^r \circ \Pi_r \circ \dot{\gamma}_{\tilde{r}}^{(\ell)} \circ \Pi_r \circ \tilde{\Gamma}_2^r + \Gamma_{2'}^r \circ \Pi_r \circ \dot{\gamma}_{\tilde{r}}^{(\ell+1)}, \\ \dot{\mathcal{K}}_3^{r(\ell+2)} &= \dot{\gamma}_{\tilde{r}}^{(\ell+1)} \circ \Pi_r \circ \tilde{\Gamma}_2^r + \tilde{\Gamma}_2^r \circ \Pi_r \circ \dot{\gamma}_{\tilde{r}}^{(\ell)} \circ \Pi_r \circ \tilde{\Gamma}_2^r \\ &\quad + \tilde{\Gamma}_2^r \circ \Pi_r \circ \dot{\gamma}_{\tilde{r}}^{(\ell+1)}. \end{aligned} \quad (24c)$$

Here, $\dot{\mathcal{K}}_1^{r(\ell+2)} \neq 0$ since $\dot{\gamma}_{\tilde{r}}^{(1)}$ appears in the middle in the central term of Eq. (11c); hence, Eq. (18c) does not apply.

Note that these equations can also be used in the context of DMF²RG [23, 24]. There, only the full vertex Γ is given as an input. While \mathcal{K}_1^r , \mathcal{K}_2^r and $\mathcal{K}_{2'}^r$ can be deduced from Γ by sending certain frequencies to infinity or using Eqs. (20), it is not possible to similarly extract \mathcal{K}_3^r in a given channel as some frequency limit of the full vertex Γ . However, the classes \mathcal{K}_3^r do not enter the right-hand sides of the flow equations (24) individually, but only the combination $\mathcal{K}_3 = \sum_r \mathcal{K}_3^r$. This is already clear from the general formulation of the mfRG flow equations, Eqs. (11). Consider, e.g., the 1ℓ contribution $\dot{\mathcal{K}}_2^{r(1)}$ of Eq. (24a). There, $\tilde{\Gamma}_2^r$ contains $\mathcal{K}_3 + \gamma_r = \mathcal{K}_3 + \sum_{r' \neq r} (\mathcal{K}_1^{r'} + \mathcal{K}_2^{r'} + \mathcal{K}_{2'}^{r'})$, and hence only requires knowledge of the full \mathcal{K}_3 . This holds equivalently for all insertions of the full vertex into flow equations at any loop order. Now, insertions of the *differentiated* vertex in loop order ℓ into the flow equations of order $\ell + 1$ and $\ell + 2$ *do* require a channel decomposition $\dot{\mathcal{K}}_3 = \sum_r \dot{\mathcal{K}}_3^r$. For example, the two-loop contribution $\dot{\mathcal{K}}_2^{r(2)}$ of Eq. (24b) contains $\dot{\gamma}_{\tilde{r}}^{(1)}$, which, by Eq. (22), involves differentiated vertices $\dot{\mathcal{K}}_3^{r' \neq r(1)}$. These *are* available via Eq. (24a). Therefore, in the DMF²RG context, one would start with \mathcal{K}_1^r , \mathcal{K}_2^r , $\mathcal{K}_{2'}^r$ and the full \mathcal{K}_3 from DMFT, compute the differentiated vertices $\dot{\mathcal{K}}_i^r$ independently (including $\dot{\mathcal{K}}_3^r$), successively insert them in higher loop orders, and eventually update \mathcal{K}_3 using $\dot{\mathcal{K}}_3 = \sum_{\ell, r} \dot{\mathcal{K}}_3^{r(\ell)}$ in each step of the flow. Note that the same reasoning also applies to the multi-boson terms M_r introduced below.

4 SBE decomposition

We now turn to the SBE decomposition. It also yields an exact, unambiguous classification of vertex diagrams, now according to their *U-reducibility* in each channel. This notion of reducibility, introduced in Ref. [15], is very analogous to *H-reducibility*, i.e., two-particle reducibility. A diagram is called *U-reducible* if it can be split into two parts by splitting apart a bare vertex U (in ways specified below) in either of the three channels. Otherwise, it is fully *U-irreducible*.

The SBE decomposition was originally formulated in terms of physical (charge, spin, and singlet pairing) channels which involve linear combinations of spin components.

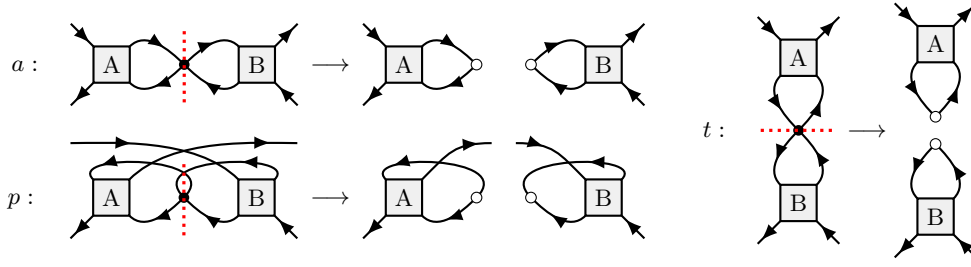


Figure 4. Illustration of U - r -reducibility, analogous to Fig. 4 of [15]. A and B can be any vertex diagram or simply $\mathbb{1}_r$.

For our purposes, it is more convenient not to use such linear combinations (the relation between both formulations is given in App. D). Moreover, the original SBE papers considered models with translational invariance, with vertices labeled by three momentum variables. We here present a generalization of the SBE decomposition applicable to models without translational invariance, requiring four position or momentum labels. Starting from the BSE, we use arguments inspired by Ref. [15] to arrive at a SBE decomposition that is closely related to the asymptotic classes of Sec. 3. This enables us to derive multiloop flow equations for the SBE constituents by arguments analogous to those of that section. In terms of notation, we follow Ref. [15] for the objects ∇_r , w_r , $\bar{\lambda}_r$, λ_r —with φ^{frr} there denoted $\varphi^{U\text{irr}}$ here—while we follow Ref. [21] for M_r and T_r (the latter instead of φ_r from Ref. [15]).

4.1 Derivation of SBE decomposition from BSE

As mentioned earlier, a vertex diagram is called two-particle reducible in a specified channel $r \in \{a, p, t\}$, or Π - r -reducible for short, if it can be split into two parts by cutting the two lines of a Π_r bubble (to be called *linking bubble*); if such a split is not possible, the diagram is called Π - r -irreducible. The two-particle reducible vertex γ_r is the sum of all Π - r -reducible diagrams. Following Ref. [15], we now introduce a further channel-specific classification criterion. A Π - r -reducible diagram is called U - r -reducible if a linking bubble Π_r has two of its legs attached to the same bare vertex in the combination $U \circ \Pi_r$ or $\Pi_r \circ U$. Then, that bare vertex U , too, constitutes a link that, when “cut”, splits the diagram into two parts. (To visualize the meaning of “cutting U ” diagrammatically, one may replace the four-leg filled dot representing U by two separate two-leg open dots, one having its two legs connected to Π_r , the other fully detached from Π_r , see Fig. 4). The lowest-order U - r -reducible contribution to γ_r is $U \circ \Pi_r \circ U$. The lowest-order term of Γ , the bare vertex U (which is Π - r -irreducible), is viewed as U - r -reducible in all three channels, corresponding to the three possible ways of splitting its four legs into two pairs of two. All U - r -reducible diagrams describe “single-boson exchange” processes, in the sense that each link U connecting two otherwise separate parts of the diagram mediates a single bosonic transfer frequency, ω_r (as defined in Fig. 3), across that link, as will become explicit below.

All vertex diagrams that are not U - r -reducible are called U - r -irreducible. These comprise all multi-boson exchange (i.e., *not* single-boson exchange) diagrams from γ_r , and all Π - r -irreducible diagrams except the bare vertex (which is trivially U - r -reducible), i.e., all diagrams from $I_r - U = R - U + \sum_{\bar{r} \neq r} \gamma_{\bar{r}}$.

We now rewrite the parquet equations in terms of U - r -reducible and U - r -irreducible constituents. We define ∇_r as the sum of all U - r -reducible diagrams, including (importantly!) the bare vertex U , and M_r as the sum of all diagrams that are Π - r -reducible but U - r -irreducible, thus describing multi-boson exchange processes. Then, the Π - r -reducible vertex γ_r , which does not include U , fulfills

$$\gamma_r = \nabla_r - U + M_r. \quad (25)$$

Inserting the decomposition (25) for γ_r into the parquet decomposition (3), we obtain the decomposition

$$\Gamma = \varphi^{U\text{irr}} + \sum_r \nabla_r - 2U, \quad (26a)$$

$$\varphi^{U\text{irr}} = R - U + \sum_r M_r, \quad (26b)$$

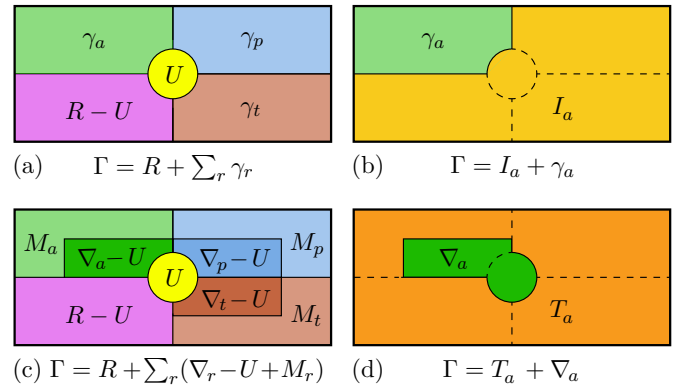


Figure 5. Venn diagrams illustrating various ways of splitting the full vertex into distinct contributions. Panel (a) depicts the parquet decomposition (3), (b) the Π - a -reducible part γ_a and its complement I_a , (c) the SBE decomposition (26) (mimicking Fig. 6 of [15]), and (d) the U - a -reducible part ∇_a and its complement T_a . For $r = p, t$, the Π - r - and U - r -reducible parts and their complements can be depicted analogously.

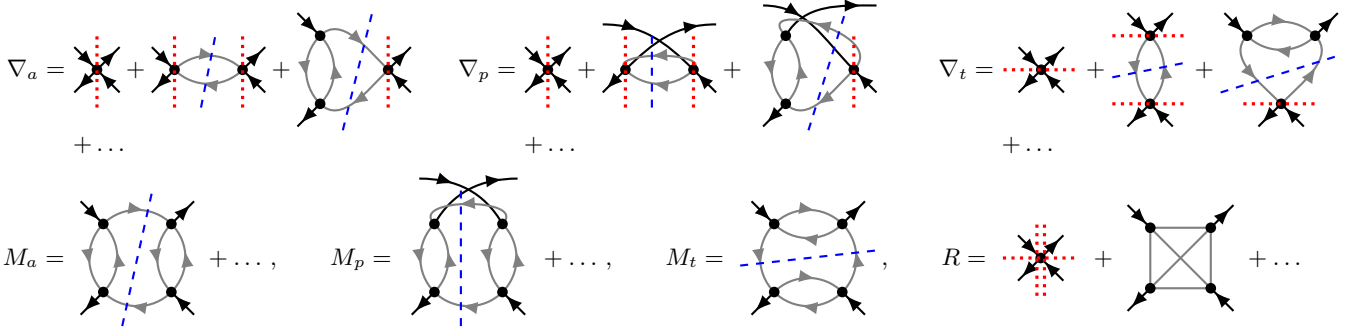


Figure 6. Low-order diagrams for ∇_r , M_r and R , illustrating Π - r -reducibility (blue dashed lines) and U - r reducibility (red dotted lines; their meaning is made explicit in Fig. 4). ∇_r contains all U - r -reducible diagrams; except for the bare vertex, they all are Π - r -reducible, too. M_a contains all diagrams that are Π - r - but not U - r -reducible. All diagrams in R are neither Π - r - nor U - r -reducible, except for the bare vertex, which is U - a -, U - p - and U - t -reducible (as indicated by three red dotted lines).

where $\varphi^{U\text{irr}}$ is the fully U -irreducible part of Γ . The U subtractions ensure that the bare vertex U , which is contained once in each ∇_r but not in $\varphi^{U\text{irr}}$, is not over-counted.

Just as γ_r , its parts ∇_r and M_r satisfy Bethe–Salpeter-type equations, which we derive next. Inserting Eq. (25) into the full vertex $\Gamma = I_r + \gamma_r$, we split it into a U - r -reducible part, ∇_r , and a U - r -irreducible remainder, T_r :

$$\Gamma = \nabla_r + T_r, \quad (27a)$$

$$T_r = I_r - U + M_r. \quad (27b)$$

The relation between various different decompositions of the full vertex implied by Eqs. (25)–(27) is illustrated in Fig. 5. Inserting Eqs. (25) and (27a) into either of the two forms of the BSE (4) for γ_r , we obtain

$$\begin{aligned} \nabla_r - U + M_r &= I_r \circ \Pi_r \circ \nabla_r + I_r \circ \Pi_r \circ T_r \\ &= \nabla_r \circ \Pi_r \circ I_r + T_r \circ \Pi_r \circ I_r. \end{aligned} \quad (28)$$

This single set of equations can be split into two separate ones, one for $\nabla_r - U$, the other for M_r , containing only U - r -reducible or only U - r -irreducible terms, respectively. The first terms on the right are clearly U - r -reducible, since they contain ∇_r . For the second terms on the right, we write I_r as the sum of U and $I_r - U$, yielding U - r -reducible and U - r -irreducible contributions, respectively. We thus obtain two separate sets of equations,

$$\begin{aligned} \nabla_r - U &= I_r \circ \Pi_r \circ \nabla_r + U \circ \Pi_r \circ T_r \\ &= \nabla_r \circ \Pi_r \circ I_r + T_r \circ \Pi_r \circ U, \end{aligned} \quad (29)$$

$$\begin{aligned} M_r &= (I_r - U) \circ \Pi_r \circ T_r \\ &= T_r \circ \Pi_r \circ (I_r - U), \end{aligned} \quad (30)$$

the latter of which corresponds to Eq. (17) in Ref. [21]. In Eqs. (29), we now bring all ∇_r contributions to the left,

$$\begin{aligned} (\mathbb{1}_r - I_r \circ \Pi_r) \circ \nabla_r &= U \circ (\mathbb{1}_r + \Pi_r \circ T_r), \\ \nabla_r \circ (\mathbb{1}_r - \Pi_r \circ I_r) &= (\mathbb{1}_r + T_r \circ \Pi_r) \circ U, \end{aligned} \quad (31)$$

and solve for ∇_r by evoking the extended BSE (7):

$$\begin{aligned} \nabla_r &= (\mathbb{1}_r + \Gamma \circ \Pi_r) \circ U \circ (\mathbb{1}_r + \Pi_r \circ T_r) \\ &= (\mathbb{1}_r + T_r \circ \Pi_r) \circ U \circ (\mathbb{1}_r + \Pi_r \circ \Gamma). \end{aligned} \quad (32)$$

These directly exhibit the U - r -reducibility of ∇_r . Equations (30) and (32) are the desired BSE for M_r and ∇_r , respectively. Together with the decomposition (27a) of the full vertex Γ , the definition $I_r = \Gamma - (\nabla_r - U + M_r)$ of all r -irreducible contributions, and definition (27b) for the auxiliary quantities T_r , they constitute a reformulation of the BSE through U - r -reducible and U - r -irreducible constituents. Some low-order contributions to ∇_r , M_r , and R are depicted diagrammatically in Fig. 6.

Having reformulated the BSE equations, we need one more step to arrive at the SBE decomposition of Ref. [15]: ∇_r must be expressed through Hedin vertices and screened interactions. To this end, we note a key structural feature of Eqs. (32): T_r is connected to the central bare vertex U through the combinations $U \circ \Pi_r \circ T_r$ or $T_r \circ \Pi_r \circ U$. When these are viewed in the r representation of Eq. (15), the bare vertex, being frequency-independent, can be pulled out in front of the frequency sum $\sum_{\nu''}$ inherent in the second \circ connector. Hence, Eqs. (32) can be expressed as

$$\begin{aligned} \nabla_r &= (\mathbb{1}_r + \Gamma \circ \Pi_r) \circ U \bullet \lambda_r \\ &= \bar{\lambda}_r \bullet U \circ (\mathbb{1}_r + \Pi_r \circ \Gamma), \end{aligned} \quad (33)$$

where $\bar{\lambda}_r$ and λ_r are the U - r -irreducible Hedin vertices (cf. Eq. (5) in Ref. [21])

$$\bar{\lambda}_r(\omega_r, \nu_r) \equiv \mathbb{1}_r + \sum_{\nu''} T_r(\omega_r, \nu_r, \nu'') \bullet \Pi_r(\omega_r, \nu''), \quad (34a)$$

$$\lambda_r(\omega_r, \nu'_r) \equiv \mathbb{1}_r + \sum_{\nu''} \Pi_r(\omega_r, \nu''_r) \bullet T_r(\omega_r, \nu''_r, \nu'_r). \quad (34b)$$

Importantly, they depend on only two frequencies, and hence are computationally less expensive than the constituents I_r , γ_r of the original parquet decomposition. (We note in passing that Hedin vertices can also be viewed as the U -irreducible, amputated parts of three-point response functions, see Eqs. (8) and (15) in Ref. [15].)

We next seek to express ∇_r as [15, 21]

$$\nabla_r = \bar{\lambda}_r \bullet w_r \bullet \lambda_r, \quad (35)$$

$$\Gamma(\omega_r, \nu_r, \nu'_r) = \varphi^{U\text{irr}}(\omega_r, \nu_r, \nu'_r) + \nabla_a(\omega_a, \nu_a, \nu'_a) + \nabla_p(\omega_p, \nu_p, \nu'_p) + \nabla_t(\omega_t, \nu_t, \nu'_t) - 2U$$

Figure 7. SBE decomposition of the vertex Γ into U - r -irreducible and U - r -reducible contributions, with $r = a, p, t$.

with two U - r -irreducible Hedin vertices sandwiching an U - r -reducible effective interaction, w_r . (The index summations implicit in Eq. (35) are made explicit in Fig. 11 in App. C.) To find w_r , we multiply Eq. (33) with the inverse Hedin vertices λ_r^{-1} or $\bar{\lambda}_r^{-1}$ (defined such that $\lambda_r \circ \lambda_r^{-1} = \mathbf{1}_r$, $\bar{\lambda}_r^{-1} \circ \bar{\lambda}_r = \mathbf{1}_r$), and use $\Gamma = \nabla_r + T_r$ to obtain

$$\begin{aligned} \nabla_r \circ \lambda_r^{-1} &= (\mathbf{1}_r + \Gamma \circ \Pi_r) \circ U = \nabla_r \circ \Pi_r \circ U + \bar{\lambda}_r \bullet U, \\ \bar{\lambda}_r^{-1} \circ \nabla_r &= U \circ (\mathbf{1}_r + \Pi_r \circ \Gamma) = U \circ \Pi_r \circ \nabla_r + U \bullet \lambda_r. \end{aligned} \quad (36)$$

We then multiply these equations with $\bar{\lambda}_r^{-1}$ or λ_r^{-1} to obtain the *effective* or *screened* interaction w_r , given by

$$\begin{aligned} w_r &= \bar{\lambda}_r^{-1} \circ \nabla_r \circ \lambda_r^{-1} \\ &= U + U \circ (\Pi_r + \Pi_r \circ \Gamma \circ \Pi_r) \circ U. \end{aligned} \quad (37)$$

It is manifestly U - r -reducible, as desired. Moreover, it depends on only a single, bosonic frequency, $w_r(\omega_r)$, since in the second term bare, frequency-independent vertices, U , sandwich expressions involving integrals over the fermionic frequencies.

Finally, we insert Eq. (35) for ∇_r into Eq. (26a) for Γ to arrive at a SBE decomposition of the full vertex akin to that proposed in Ref. [15]:

$$\Gamma = \varphi^{U\text{irr}} + \sum_r \bar{\lambda}_r \bullet w_r \bullet \lambda_r - 2U. \quad (38)$$

Figure 7 depicts it diagrammatically, using wiggly lines for screened interactions and triangles, with two fermionic legs and one wiggly bosonic leg, for Hedin vertices.

4.2 Relation between SBE constituents and asymptotic classes

The asymptotic classes and SBE constituents are closely related. This is not surprising since the properties of both follow from the assumption that the bare vertex contains no frequency dependence, except for frequency conservation. For convenience, we collect these relations below.

Comparison of Eqs. (20a), (21), and (37) yields

$$w_r(\omega_r) = U + \mathcal{K}_1^r(\omega_r) = U + U \bullet \chi_r(\omega_r) \bullet U. \quad (39)$$

The screened interaction w_r is therefore mediated by the bosonic fluctuations described by the susceptibility χ_r .

The Hedin vertices, $\bar{\lambda}_r$ and λ_r , describe the coupling of fermions to these bosonic fluctuations. Using Eqs. (20b), (20c), (35), and (37), we can write the products of Hedin vertices and the screened interaction as

$$\bar{\lambda}_r \bullet w_r = U + \Gamma \circ \Pi_r \circ U = U + \mathcal{K}_1^r + \mathcal{K}_2^r, \quad (40a)$$

$$w_r \bullet \lambda_r = U + U \circ \Pi_r \circ \Gamma = U + \mathcal{K}_1^r + \mathcal{K}_2^r. \quad (40b)$$

Inserting Eq. (39) for $U + \mathcal{K}_1^r$, and defining w_r^{-1} through $w_r \bullet w_r^{-1} = w_r^{-1} \bullet w_r = \mathbf{1}_r$, we thus obtain

$$\bar{\lambda}_r = \mathbf{1}_r + \mathcal{K}_2^r \bullet w_r^{-1}, \quad \lambda_r = \mathbf{1}_r + w_r^{-1} \bullet \mathcal{K}_2^r, \quad (41)$$

which, when inserted into Eq. (35), yields

$$\begin{aligned} \nabla_r &= (\mathbf{1}_r + \mathcal{K}_2^r \bullet w_r^{-1}) \bullet w_r \bullet (\mathbf{1}_r + w_r^{-1} \bullet \mathcal{K}_2^r) \\ &= U + \mathcal{K}_1^r + \mathcal{K}_2^r + \mathcal{K}_2^r \bullet w_r^{-1} \bullet \mathcal{K}_2^r. \end{aligned} \quad (42)$$

Through the last term, $\mathcal{K}_2^r \bullet w_r^{-1} \bullet \mathcal{K}_2^r$, ∇_r includes a part of \mathcal{K}_3^r which can be fully expressed through functions that each depend on at most two frequencies. M_r contains the remaining part of \mathcal{K}_3^r , which must be explicitly parametrized through three frequencies and thus is numerically most expensive. A recent study of the Hubbard model showed that M_r is strongly localized in frequency space, particularly in the strong-coupling regime [22]. This allows for a cheaper numerical treatment of the vertex part truly depending on three frequencies and constitutes the main computational advantage of the SBE decomposition.

Equations (39) to (42) fully express the SBE constituents through asymptotic classes. Analogous results were obtained by similar arguments in App. A of Ref. [22]. In Ref. [15], it was also shown that $\bar{\lambda}_r = \lambda_r$ for SU(2) spin and time-reversal symmetry.

Conversely, the asymptotic classes can also be expressed fully through the SBE constituents. Using Eqs. (17), (25), (39), and (41), one finds

$$\mathcal{K}_1^r = w_r - U \quad (43a)$$

$$\mathcal{K}_2^r = (\bar{\lambda}_r - \mathbf{1}_r) \bullet w_r, \quad (43b)$$

$$\mathcal{K}_2^r = w_r \bullet (\lambda_r - \mathbf{1}_r), \quad (43c)$$

$$\mathcal{K}_3^r = M_r + (\bar{\lambda}_r - \mathbf{1}_r) \bullet w_r \bullet (\lambda_r - \mathbf{1}_r). \quad (43d)$$

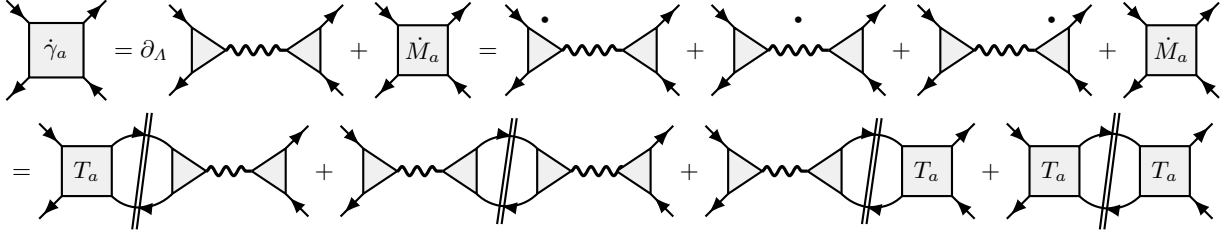


Figure 8. SBE decomposition of the left and right sides of the 1ℓ flow equation (11a) (Fig. 2) in the a channel. The first line depicts Eq. (46), the second Eq. (47). Equating terms with matching structure yields Eq. (48a), depicted in Fig. 9, first line.

Moreover, Eqs. (19b), (19c), (27a), and (40) imply

$$\Gamma_2^r = \bar{\lambda}_r \bullet w_r, \quad (44a)$$

$$\Gamma_{2'}^r = w_r \bullet \lambda_r, \quad (44b)$$

$$\bar{\Gamma}_2^r = \bar{\lambda}_r \bullet w_r \bullet (\lambda_r - \mathbf{1}_r) + T_r \quad (44c)$$

$$\bar{\Gamma}_{2'}^r = (\bar{\lambda}_r - \mathbf{1}_r) \bullet w_r \bullet \lambda_r + T_r. \quad (44d)$$

For the latter two equations, we used Eq. (27a) in the form $\Gamma = \bar{\lambda}_r \bullet w_r \bullet \lambda_r + T_r$. Equivalently, using the definitions of the Hedin vertices in Eq. (34), \mathcal{K}_2^r , \mathcal{K}_3^r , and Eqs. (44) can be expressed as

$$\mathcal{K}_2^r = T_r \circ \Pi_r \circ w_r, \quad (45a)$$

$$\mathcal{K}_{2'}^r = w_r \circ \Pi_r \circ T_r, \quad (45b)$$

$$\mathcal{K}_3^r = M_r + T_r \circ \Pi_r \circ w_r \circ \Pi_r \circ T_r, \quad (45c)$$

$$\Gamma_2^r = w_r + T_r \circ \Pi_r \circ w_r, \quad (45d)$$

$$\Gamma_{2'}^r = w_r + w_r \circ \Pi_r \circ T_r, \quad (45e)$$

$$\bar{\Gamma}_2^r = T_r + w_r \circ \Pi_r \circ T_r + T_r \circ \Pi_r \circ w_r \circ \Pi_r \circ T_r, \quad (45f)$$

$$\bar{\Gamma}_{2'}^r = T_r + T_r \circ \Pi_r \circ w_r + T_r \circ \Pi_r \circ w_r \circ \Pi_r \circ T_r. \quad (45g)$$

4.3 mfRG equations for SBE

We are now ready to derive mfRG flow equations for the SBE constituents—the main goal of this work. Our strategy is to insert the SBE decomposition of Eqs. (25) and (26) into the mfRG flow equations (11) for the Π_r -reducible vertices γ_r , similar to the derivation of the mfRG flow equations for the asymptotic classes in Sec. 3.3. (An alternative derivation directly from parquet-like equations for the SBE constituents is given in App. E.)

We begin by differentiating the decomposition of the Π_r -reducible vertex $\gamma_r = \bar{\lambda}_r \bullet w_r \bullet \lambda_r - U + M_r$ [Eq. (25)] w.r.t. the flow parameter. Since $\dot{U} = 0$ (the bare vertex does not depend on the regulator), we obtain

$$\dot{\gamma}_r = \dot{\bar{\lambda}}_r \bullet w_r \bullet \lambda_r + \bar{\lambda}_r \bullet \dot{w}_r \bullet \lambda_r + \bar{\lambda}_r \bullet w_r \bullet \dot{\lambda}_r + \dot{M}_r. \quad (46)$$

The loop expansion $\dot{\gamma}_r = \sum_{\ell} \dot{\gamma}_r^{(\ell)}$ implies similar expansions for \dot{w}_r , $\dot{\bar{\lambda}}_r$, $\dot{\lambda}_r$ and \dot{M}_r . Their constituents can be found from the mfRG flow equations (11) for $\dot{\gamma}_r^{(\ell)}$ at order ℓ , by inserting the decomposition of the full vertex, $\Gamma = \bar{\lambda}_r \bullet w_r \bullet \lambda_r + T_r$ [Eq. (27a)] on the right of Eqs. (11).

The 1ℓ flow equation (11a) of $\dot{\gamma}_r^{(1)}$ has four contributions (depicted diagrammatically for $\gamma_a^{(1)}$ in Fig. 8):

$$\begin{aligned} \dot{\gamma}_r^{(1)} &= (\bar{\lambda}_r \bullet w_r \bullet \lambda_r + T_r) \circ \dot{\Pi}_r \circ (\bar{\lambda}_r \bullet w_r \bullet \lambda_r + T_r) \\ &= T_r \circ \dot{\Pi}_r \circ \bar{\lambda}_r \bullet w_r \bullet \lambda_r \\ &\quad + \bar{\lambda}_r \bullet w_r \bullet \lambda_r \circ \dot{\Pi}_r \circ \bar{\lambda}_r \bullet w_r \bullet \lambda_r \\ &\quad + \bar{\lambda}_r \bullet w_r \bullet \lambda_r \circ \dot{\Pi}_r \circ T_r + T_r \circ \dot{\Pi}_r \circ T_r. \end{aligned} \quad (47)$$

By matching terms in Eqs. (46) and (47) containing factors of $\bar{\lambda}_r$ and λ_r or not, we obtain the 1ℓ SBE flow:

$$\begin{aligned} \dot{\bar{\lambda}}_r^{(1)} &= T_r \circ \dot{\Pi}_r \circ \bar{\lambda}_r, \\ \dot{w}_r^{(1)} &= w_r \bullet \lambda_r \circ \dot{\Pi}_r \circ \bar{\lambda}_r \bullet w_r, \\ \dot{\lambda}_r^{(1)} &= \lambda_r \circ \dot{\Pi}_r \circ T_r, \\ \dot{M}_r^{(1)} &= T_r \circ \dot{\Pi}_r \circ T_r. \end{aligned} \quad (48a)$$

This reproduces the 1ℓ SBE flow derived in Ref. [22] [their Eq. (18)]. The higher-loop terms can be found similarly from $\dot{\gamma}_r^{(2)}$ and $\dot{\gamma}_r^{(\ell+2)}$ of Eqs. (11b) and (11c). For each loop order ℓ , the $\dot{\gamma}_r^{(\ell)}$ factors on the right side of these equations can be expressed through the already known flow of $\dot{w}_r^{(\ell)}$, $\dot{\bar{\lambda}}_r^{(\ell)}$, $\dot{\lambda}_r^{(\ell)}$ and $\dot{M}_r^{(\ell)}$. We obtain the flow equations ($\ell+2 \geq 3$)

$$\begin{aligned} \dot{\bar{\lambda}}_r^{(2)} &= \dot{\gamma}_r^{(1)} \circ \Pi_r \circ \bar{\lambda}_r, \\ \dot{w}_r^{(2)} &= 0, \\ \dot{\lambda}_r^{(2)} &= \lambda_r \circ \Pi_r \circ \dot{\gamma}_r, \\ \dot{M}_r^{(2)} &= \dot{\gamma}_r^{(1)} \circ \Pi_r \circ T_r + T_r \circ \Pi_r \circ \dot{\gamma}_r^{(1)}, \end{aligned} \quad (48b)$$

$$\begin{aligned} \dot{\bar{\lambda}}_r^{(\ell+2)} &= \dot{\gamma}_r^{(\ell+1)} \circ \Pi_r \circ \bar{\lambda}_r + T_r \circ \Pi_r \circ \dot{\gamma}_r^{(\ell)} \circ \Pi_r \circ \bar{\lambda}_r, \\ \dot{w}_r^{(\ell+2)} &= w_r \bullet \lambda_r \circ \Pi_r \circ \dot{\gamma}_r^{(\ell)} \circ \Pi_r \circ \bar{\lambda}_r \bullet w_r, \\ \dot{\lambda}_r^{(\ell+2)} &= \lambda_r \circ \Pi_r \circ \dot{\gamma}_r^{(\ell)} \circ \Pi_r \circ T_r + \lambda_r \circ \Pi_r \circ \dot{\gamma}_r^{(\ell+1)}, \\ \dot{M}_r^{(\ell+2)} &= \dot{\gamma}_r^{(\ell+1)} \circ \Pi_r \circ T_r + T_r \circ \Pi_r \circ \dot{\gamma}_r^{(\ell)} \circ \Pi_r \circ T_r \\ &\quad + T_r \circ \Pi_r \circ \dot{\gamma}_r^{(\ell+1)}. \end{aligned} \quad (48c)$$

Here $\dot{\gamma}_r^{(\ell)}$, required for the flow equations in loop order $\ell+1$ and $\ell+2$, can directly be constructed from the SBE constituents using Eq. (46). The multiloop SBE flow equations (48) are the most important result of this work.

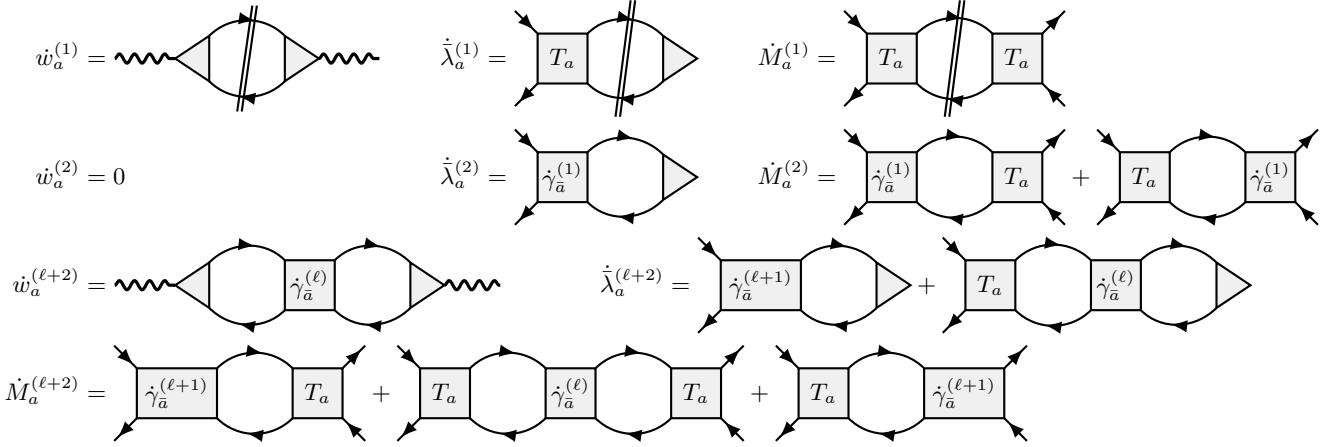


Figure 9. Multiloop flow equations (48) for the constituents of the SBE decomposition in the a channel.

For the a channel, they are depicted diagrammatically in Fig. 9. Equations (48) can be condensed into more compact ones, giving the full flow (summed over all loop orders, $\dot{w}_r = \sum_{\ell \geq 1} \dot{w}_r^{(\ell)}$, etc.) of the SBE ingredients. These are given in App. E. The multiloop flow equation for the self-energy can be found in Refs. [5, 7].

Since the asymptotic classes and SBE constituents are closely related, the same is true for their mRG flow. Indeed, it is straightforward to derive the mRG SBE flow equations (48) from the flow equations (24) for $\dot{\mathcal{K}}_i^r$. We briefly indicate the strategy, without presenting all details.

We differentiate the equations (43) expressing \mathcal{K}_i^r through SBE constituents, and subsequently use Eqs. (34) to eliminate $\bar{\lambda}_r - \mathbf{1}_r$ and $\lambda_r - \mathbf{1}_r$. Thereby, we obtain

$$\dot{\mathcal{K}}_1^r = \dot{w}_r \quad (49a)$$

$$\dot{\mathcal{K}}_2^r = \dot{\bar{\lambda}}_r \cdot w_r + T_r \circ \Pi_r \circ \dot{w}_r, \quad (49b)$$

$$\dot{\mathcal{K}}_{2'}^r = \dot{w}_r \circ \Pi_r \circ T_r + w_r \cdot \dot{\lambda}_r, \quad (49c)$$

$$\begin{aligned} \dot{\mathcal{K}}_3^r &= \dot{\bar{\lambda}}_r \cdot w_r \circ \Pi_r \circ T_r + T_r \circ \Pi_r \circ \dot{w}_r \circ \Pi_r \circ T_r \\ &+ T_r \circ \Pi_r \circ w_r \cdot \dot{\lambda}_r + \dot{M}_r. \end{aligned} \quad (49d)$$

Now, we use Eqs. (24) to express the $\dot{\mathcal{K}}_i^r$ on the left through $\Gamma_2^r, \bar{\Gamma}_2^r, \bar{\Gamma}_2^r, \bar{\Gamma}_2^r$, and Eqs. (44) to express the latter through SBE constituents. By matching terms on the left and right in each loop order, we obtain flow equations for $\dot{w}^{(\ell)}$, $\dot{\bar{\lambda}}_r^{(\ell)}$, $\dot{\lambda}_r^{(\ell)}$ and $\dot{M}_r^{(\ell)}$. For example, at 1ℓ order, Eqs. (24a) and (49a) for $\dot{\mathcal{K}}_1^r$ yield

$$\dot{w}_r^{(1)} = \Gamma_2^r \circ \dot{\Pi}_r \circ \Gamma_2^r = w_r \cdot \lambda_r \circ \dot{\Pi}_r \circ \bar{\lambda}_r \cdot w_r, \quad (50)$$

consistent with Eq. (48a). Similarly, for $\dot{\mathcal{K}}_2^r$, we obtain

$$\begin{aligned} \dot{\bar{\lambda}}_r^{(1)} \cdot w_r + T_r \circ \Pi_r \circ \dot{w}_r^{(1)} &= \bar{\Gamma}_2^r \circ \dot{\Pi}_r \circ \Gamma_2^r \\ &= T_r \circ \dot{\Pi}_r \circ \bar{\lambda}_r \cdot w_r + T_r \circ \Pi_r \circ w_r \cdot \lambda_r \circ \dot{\Pi}_r \circ \bar{\lambda}_r \cdot w_r. \end{aligned} \quad (51)$$

The second terms on the left and right cancel due to Eq. (50). The remaining terms, right-multiplied by w_r^{-1} ,

yield $\dot{\bar{\lambda}}_r^{(1)} = T_r \circ \dot{\Pi}_r \circ \bar{\lambda}_r$, consistent with (48a). All of the equations (48) can be derived in this manner.

5 Conclusions and outlook

The SBE decomposition of the four-point vertex was originally introduced in Hubbard-like models respecting SU(2) symmetry and was written in terms of physical (e.g., spin and charge) channels [15]. In this work, we formulated the SBE decomposition without specifying the structure of non-frequency arguments (such as position or momentum, spin, etc.) starting from the BSE for general fermionic models. The only restriction on the structure of the bare vertex U is that, apart from being frequency-conserving, it is otherwise constant in frequency. Our formulation can thus be used as a starting point for a rather general class of models. It is straightforward to extend our formulation to the Keldysh formalism, or to other types of particle fields such as bosons or real fermions.

We gave a detailed discussion of the relation between two decompositions of the full vertex, involving the asymptotic classes \mathcal{K}_i^r , or the SBE constituents, M_r and $\nabla_r = \bar{\lambda}_r \cdot w_r \cdot \lambda_r$. The latter have a transparent interpretation through bosonic exchange fluctuations and Hedin vertices, describing effective interactions between these bosonic fluctuations and two fermions. We showed that the two decompositions are closely related and presented detailed formulas linking their constituents. As our main result, we derived multiloop flow equations for both decompositions. Thereby, we presented the multiloop generalization of the 1ℓ SBE flow of Ref. [22] and also provided a unified formulation for the mRG treatment of the two vertex decompositions.

A numerical study of the mRG SBE flow for relevant model systems, such as the single-impurity Anderson model or the Hubbard model, is left for future work. Below, we outline some open questions to be addressed.

The numerically most expensive SBE constituent is the fully U -irreducible vertex $\varphi^{U_{\text{irr}}}$, involving the U - r -

irreducible contributions M_r , because these all depend on three frequency arguments. One may hope that, for certain applications, it might suffice to neglect $\varphi^{U_{\text{irr}}}$ (as done in Ref. [18] for a DMFT treatment of the Hubbard model), or to treat it in a cheap fashion, e.g., by not keeping track of its full frequency dependence or by not letting it flow (cf. Ref. [22]). This spoils the parquet two-particle self-consistency while retaining SBE self-consistency. It is an interesting open question which of the main qualitative features of the parquet solution remain intact this way.

One formal feature, namely regulator independence, can be identified *a priori* for the case that the SBE multiloop flow equations are simplified by setting $\varphi^{U_{\text{irr}}} = 0$ and $\dot{M}_r = 0$ throughout the flow. Then, the right side of the simplified flow equations still constitutes a total derivative. Therefore, if loop convergence can be achieved when integrating these simplified flow equations, the results will be regulator independent, just as for a mfRG flow with $\varphi^{U_{\text{irr}}} = \sum_r M_r$ reproducing the parquet approximation.

Even if it turns out that a full treatment of $\varphi^{U_{\text{irr}}}$ is required for capturing essential qualitative features of the vertex, this might still be numerically cheaper than a full treatment of \mathcal{K}_3 . The reason is that each \mathcal{K}_3^r contains a contribution, the $\mathcal{K}_2^r \cdot w_r^{-1} \cdot \mathcal{K}_2^r$ term in Eq. (42), which is included not in M_r but in ∇_r , and parametrized through the numerically cheaper Hedin vertices and effective interactions. If these terms decay comparatively slowly with frequency, their treatment via the \mathcal{K}_i^r decomposition would be numerically expensive, and the SBE decomposition could offer a numerically cheaper alternative. A systematic comparison of the numerical costs required to compute the multiloop flow of the two decompositions should thus be a main goal of future work.

Acknowledgments We thank F. Krien and N. Ritz for critical reading of the manuscript. This research is part of the Munich Quantum Valley, which is supported by the Bavarian state government with funds from the Hightech Agenda Bayern Plus. We acknowledge funding for M.G. from the International Max Planck Research School for Quantum Science and Technology (IMPRS-QST), for A.G. and J.v.D. from the Deutsche Forschungsgemeinschaft under Germany's Excellence Strategy EXC-2111 (Project No. 390814868), and for F.B.K. from the Alexander von Humboldt Foundation through the Feodor Lynen Fellowship.

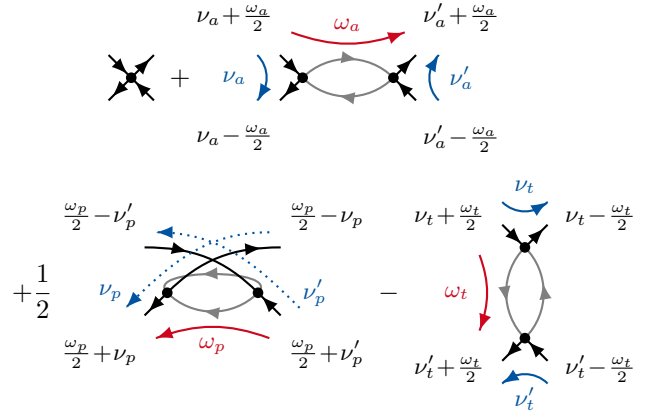
Author contributions

E.W., M.G., A.G., and F.B.K. contributed to the derivation of the presented equations. All authors jointly prepared the manuscript.

A Diagrammatic definition of \mathcal{K}_1 , \mathcal{K}_2 , \mathcal{K}_3

We illustrate the channel-dependent frequency parametrizations of the vertex (Fig. 3) in second-order per-

turbation theory:



The bosonic frequency ω_r is “transferred” through the bubble in which each diagram is reducible, while the fermionic frequencies ν_r, ν'_r parametrize the frequency dependence on each side of the bubble. Evidently, the internal propagator lines only depend on the bosonic transfer frequency of the corresponding channel (and the internal integration frequency). The external fermionic frequency ν_r flows in and out at the same bare vertex, and so does ν'_r at another bare vertex, such that the value of each diagram is independent of ν_r, ν'_r . This notion can be generalized, leading to the decomposition of each Π - r -reducible vertex γ_r into four different asymptotic classes, $\mathcal{K}_1^r + \mathcal{K}_2^r + \mathcal{K}_3^r + \mathcal{K}_3^r$, depicted diagrammatically in Fig. 10. A formal definition is given by Eqs. (18) in the main text.

B Susceptibilities

In the following, we show how the susceptibilities defined in Eq. (21b) are related to physical charge, spin, and pairing susceptibilities. To this end, we focus on models with a local (momentum-independent) bare interaction, which has only spin degrees of freedom subject to the Pauli principle. In the a and t channel, Eq. (21a) then reads

$$\mathcal{K}_1^{a;\sigma\sigma'|\sigma\sigma'} = U^{\sigma\bar{\sigma}|\bar{\sigma}'\sigma'} \chi_a^{\bar{\sigma}'\bar{\sigma}|\bar{\sigma}'\bar{\sigma}} U^{\bar{\sigma}\sigma'|\sigma\bar{\sigma}}, \quad (53a)$$

$$\mathcal{K}_1^{t;\sigma\sigma'|\sigma\sigma'} = U^{\bar{\sigma}'\sigma'|\bar{\sigma}'\sigma'} \chi_t^{\bar{\sigma}\bar{\sigma}'|\bar{\sigma}\bar{\sigma}'} U^{\sigma\bar{\sigma}|\sigma\bar{\sigma}}. \quad (53b)$$

We furthermore specify $U^{\sigma\bar{\sigma}|\bar{\sigma}'\sigma'} = u(\delta_{\sigma\sigma'} - \delta_{\sigma\bar{\sigma}'})$, with the (scalar) bare interaction strength u . With SU(2) symmetry, $\chi_r^{\sigma_1\sigma'_1|\sigma_2\sigma'_2} = \chi_r^{\bar{\sigma}_1\bar{\sigma}'_1|\bar{\sigma}_2\bar{\sigma}'_2}$, Eq. (53) thus simplifies to

$$\chi_{a/t}^{\sigma\sigma'|\sigma\sigma'} = \mathcal{K}_1^{a/t;\sigma\sigma'|\sigma\sigma'} / u^2. \quad (54)$$

In the p channel, we have

$$\mathcal{K}_1^{p;\sigma\sigma'|\sigma\sigma'} = \sum_{\sigma_1\sigma_2} U^{\sigma\sigma'|\sigma_1\bar{\sigma}_1} \chi_p^{\sigma_1\bar{\sigma}_1|\sigma_2\bar{\sigma}_2} U^{\sigma_2\bar{\sigma}_2|\sigma\sigma'} \quad (55a)$$

$$= U^{\sigma\sigma'|\sigma\sigma'} \tilde{\chi}_p^{\sigma\sigma'|\sigma\sigma'} U^{\sigma\sigma'|\sigma\sigma'}. \quad (55b)$$

$$\begin{aligned}
\gamma_a(\omega_a, \nu_a, \nu'_a) &= \mathcal{K}_1^a(\omega_a) + \mathcal{K}_2^a(\omega_a, \nu_a) + \mathcal{K}_{2'}^a(\omega_a, \nu'_a) + \mathcal{K}_3^a(\omega_a, \nu_a, \nu'_a), \\
\gamma_p(\omega_p, \nu_p, \nu'_p) &= \mathcal{K}_1^p(\omega_p) + \mathcal{K}_2^p(\omega_p, \nu_p) + \mathcal{K}_{2'}^p(\omega_p, \nu'_p) + \mathcal{K}_3^p(\omega_p, \nu_p, \nu'_p), \\
\gamma_t(\omega_t, \nu_t, \nu'_t) &= \mathcal{K}_1^t(\omega_t) + \mathcal{K}_2^t(\omega_t, \nu_t) + \mathcal{K}_{2'}^t(\omega_t, \nu'_t) + \mathcal{K}_3^t(\omega_t, \nu_t, \nu'_t).
\end{aligned}$$

Figure 10. Illustration of the decomposition of the two-particle reducible vertices γ_r into asymptotic classes, $\mathcal{K}_1^r + \mathcal{K}_2^r + \mathcal{K}_{2'}^r + \mathcal{K}_3^r$.

Here, the second line (55b) follows from SU(2) and crossing symmetry. It employs

$$\begin{aligned}
\tilde{\chi}_p(\omega_p) &= \sum_{\nu_p''} \tilde{H}_p(\omega_p, \nu_p'') \\
&+ \sum_{\nu_p, \nu_p'} \tilde{H}_p(\omega_p, \nu_p) \cdot \Gamma(\omega_p, \nu_p, \nu_p') \cdot \tilde{H}_p(\omega_p, \nu_p'),
\end{aligned} \quad (56)$$

where $\tilde{H}_{p;34|3'4'} = G_{3|3'}G_{4|4'} = 2\Pi_{p;34|3'4'}$ does not include a prefactor 1/2 (introduced in Eq. (5b) in order to avoid double counting within internal spin sums), since there are no spin sums in Eq. (55b). (This definition of the p susceptibility agrees with the related literature, e.g., Ref. [28].) With $U^{\sigma\sigma'|\sigma\sigma'} = -u\delta_{\sigma\sigma'}$, this allows us to write

$$\tilde{\chi}_p^{\sigma\sigma'|\sigma\sigma'} = \delta_{\sigma\sigma'} \mathcal{K}_1^{p;\sigma\sigma'|\sigma\sigma'} / u^2, \quad (57)$$

in analogy to Eq. (54).

The relation between these “diagrammatic” susceptibilities χ_r and their “physical” counterparts can be made explicit by means of the bilinears

$$\rho_{\sigma\sigma'} = \bar{c}_\sigma c_{\sigma'}, \quad \delta\rho_{\sigma\sigma'} = \rho_{\sigma\sigma'} - \langle \rho_{\sigma\sigma'} \rangle \delta_{\sigma\sigma'} \quad (58a)$$

$$\rho_{\sigma\sigma'}^- = c_\sigma c_{\sigma'}, \quad \rho_{\sigma\sigma'}^+ = \bar{c}_{\sigma'} \bar{c}_\sigma. \quad (58b)$$

Then, we have in the imaginary-time domain

$$\chi_a^{\sigma\sigma'|\sigma\sigma'}(\tau) = -\langle \delta\rho_{\sigma'\sigma}(\tau) \delta\rho_{\sigma\sigma'}(0) \rangle, \quad (59a)$$

$$\tilde{\chi}_p^{\sigma\sigma'|\sigma\sigma'}(\tau) = \langle \rho_{\sigma\sigma'}^-(\tau) \rho_{\sigma\sigma'}^+(0) \rangle, \quad (59b)$$

$$\chi_t^{\sigma\sigma'|\sigma\sigma'}(\tau) = \langle \delta n_\sigma(\tau) \delta n_{\sigma'}(0) \rangle. \quad (59c)$$

with $n_\sigma = \rho_{\sigma\sigma}$. Choosing the spin arguments as $\chi_r^{\uparrow\downarrow} = \chi_r^{\uparrow\downarrow|\uparrow\downarrow}$, we furthermore get

$$\chi_a^{\uparrow\downarrow}(\tau) = -\langle S_-(\tau) S_+ \rangle, \quad (60a)$$

$$\tilde{\chi}_p^{\uparrow\downarrow}(\tau) = \langle \Delta_{\text{si}}(\tau) \Delta_{\text{si}}^\dagger(0) \rangle, \quad (60b)$$

$$\chi_t^{\uparrow\downarrow}(\tau) = \langle \delta n_\uparrow(\tau) \delta n_\downarrow(0) \rangle. \quad (60c)$$

Hence, $\chi_a^{\uparrow\downarrow}$ describes spin fluctuations ($S_- = \bar{c}_\downarrow c_\uparrow$, $S_+ = \bar{c}_\uparrow c_\downarrow$) and $\tilde{\chi}_p^{\uparrow\downarrow}$ singlet pairing fluctuations ($\Delta_{\text{si}} = c_\uparrow c_\downarrow$). By SU(2) spin symmetry, $\frac{1}{2}\chi_a^{\uparrow\downarrow}(\tau) = -\langle S_z(\tau) S_z \rangle$, with $S_z = \frac{1}{2}(n_\uparrow - n_\downarrow) = \frac{1}{2}(\delta n_\uparrow - \delta n_\downarrow)$. It then follows that

$$\begin{aligned}
\chi_t^{\uparrow\downarrow}(\tau) - \frac{1}{2}\chi_a^{\uparrow\downarrow}(\tau) &= \frac{1}{2}(\langle \delta n_\uparrow(\tau) \delta n_\uparrow \rangle + \langle \delta n_\uparrow(\tau) \delta n_\downarrow \rangle) \\
&= \frac{1}{4}\langle \delta n(\tau) \delta n \rangle
\end{aligned} \quad (61)$$

describes charge fluctuations with $n = n_\uparrow + n_\downarrow$.

C Diagrammatic illustration of SBE objects

Figure 11 illustrates which part of the U - r -reducible diagrams ∇_r belong to the Hedin vertices $\bar{\lambda}_r, \lambda_r$ and which parts belong to the effective screened interactions w_r (for exemplary low-order diagrams see Figure 6).

D Relation to SBE formulation in physical channels

The SBE decomposition was originally defined in terms of the charge, spin, and singlet pairing channels [15]. These

$$\begin{aligned}
& \text{Diagram 1: } \bar{\lambda}_a \cdot w_a \cdot \lambda_a = \bar{\lambda}_a \cdot U \cdot \lambda_a + \bar{\lambda}_a \cdot \mathcal{K}_1^a \cdot \lambda_a, \quad \text{e.g. } \bar{\lambda}_a \in \bar{\lambda}_a, \mathcal{K}_1^a \subset w_a, \lambda_a \in \lambda_a \\
& = \nabla_{a;1'2'|12}(\omega_a, \nu_a, \nu'_a) = (\bar{\lambda}_a \cdot w_a \cdot \lambda_a)_{1'2'|12}(\omega_a, \nu_a, \nu'_a) = \bar{\lambda}_{a;1'4|3'2}(\omega_a, \nu_a) w_{a;3'4'|34}(\omega_a) \lambda_{a;32'|14'}(\omega_a, \nu'_a) \\
& \text{Diagram 2: } \bar{\lambda}_p \cdot w_p \cdot \lambda_p = \bar{\lambda}_p \cdot U \cdot \lambda_p + \bar{\lambda}_p \cdot \mathcal{K}_1^p \cdot \lambda_p, \quad \text{e.g. } \bar{\lambda}_p \in \bar{\lambda}_p, \mathcal{K}_1^p \subset w_p, \lambda_p \in \lambda_p \\
& = \nabla_{p;1'2'|12}(\omega_p, \nu_p, \nu'_p) = (\bar{\lambda}_p \cdot w_p \cdot \lambda_p)_{1'2'|12}(\omega_p, \nu_p, \nu'_p) = \bar{\lambda}_{p;1'2'|3'4'}(\omega_p, \nu_p) w_{p;3'4'|34}(\omega_p) \lambda_{p;34|12}(\omega_p, \nu'_p) \\
& \text{Diagram 3: } \bar{\lambda}_t \cdot w_t \cdot \lambda_t = \bar{\lambda}_t \cdot U \cdot \lambda_t + \bar{\lambda}_t \cdot \mathcal{K}_1^t \cdot \lambda_t, \quad \text{e.g. } \bar{\lambda}_t \in \bar{\lambda}_t, \mathcal{K}_1^t \subset w_t, \lambda_t \in \lambda_t \\
& = \nabla_{t;1'2'|12}(\omega_t, \nu_t, \nu'_t) = (\bar{\lambda}_t \cdot w_t \cdot \lambda_t)_{1'2'|12}(\omega_t, \nu_t, \nu'_t) = \bar{\lambda}_{t;42'|3'2}(\omega_t, \nu_t) w_{t;4'3'|34}(\omega_t) \lambda_{t;1'3|14'}(\omega_t, \nu'_t)
\end{aligned}$$

Figure 11. Illustration of the structure of ∇_r using $w_r = U + \mathcal{K}_1^r$ [Eq. (39)], including an exemplary sixth-order diagram. While $\bar{\lambda}_r$, w_r , λ_r factorize w.r.t. their frequency dependence (since they are connected by bare vertices in ∇_r), they are viewed as four-point objects w.r.t. the other quantum numbers [the internal indices 3, 3', 4, 4' have to be summed over, cf. Eq. (6)].

involve specific linear combinations of the spin components, chosen to diagonalize the spin structure in the BSE for SU(2)-symmetric systems [9]. Assuming SU(2) spin symmetry, we show below how these “physical” SBE channels are related to the “diagrammatic” SBE channels used in the main text.

By spin conservation, each incoming spin $\sigma \in \{\uparrow, \downarrow\}$ must also come out of a vertex. The nonzero components thus are

$$\Gamma^{\sigma\bar{\sigma}} = \Gamma^{\sigma\bar{\sigma}|\sigma\bar{\sigma}}, \quad \hat{\Gamma}^{\sigma\bar{\sigma}} = \Gamma^{\sigma\bar{\sigma}|\bar{\sigma}\sigma}, \quad \Gamma^{\sigma\sigma} = \Gamma^{\sigma\sigma|\sigma\sigma}. \quad (62)$$

Furthermore, crossing symmetry relates $\Gamma^{\uparrow\downarrow}$ and $\hat{\Gamma}^{\uparrow\downarrow}$, and SU(2)-spin symmetry yields $\Gamma^{\sigma\sigma} = \Gamma^{\sigma\bar{\sigma}} + \hat{\Gamma}^{\sigma\bar{\sigma}}$ [39].

On the level of the full vertex, we define the charge, spin, and singlet or triplet pairing channels as

$$\Gamma^{\text{ch/sp}} = \Gamma^{\uparrow\uparrow} \pm \Gamma^{\uparrow\downarrow}, \quad \Gamma^{\text{tr/si}} = \Gamma^{\uparrow\downarrow} \pm \hat{\Gamma}^{\uparrow\downarrow}. \quad (63)$$

This notation carries over to all vertex objects like ∇_r^α , λ_r^α and w_r^α , with α denoting ch, sp, si, or tr.

The bare vertex has $U^{\uparrow\uparrow} = 0$ and $U^{\uparrow\downarrow} = -\hat{U}^{\uparrow\downarrow}$, so that

$$U^{\text{ch/sp}} = U^{\uparrow\uparrow} \pm U^{\uparrow\downarrow} = \pm U^{\uparrow\downarrow}, \quad (64a)$$

$$U^{\text{si}} = U^{\uparrow\downarrow} - \hat{U}^{\uparrow\downarrow} = 2U^{\uparrow\downarrow}. \quad (64b)$$

The bare interaction U^{tr} in the triplet pairing channel vanishes and does not give a U -reducible contribution [15].

We now show that if the constituents of the SBE decomposition Eq. (38) are expressed through the physical charge and spin components (ch, sp) rather than the diagrammatic components ($\uparrow\uparrow$, $\uparrow\downarrow$) used here, one indeed obtains the original form of the SBE decomposition depicted in Fig. 1 of Ref. [15].

This is trivial to see for the fully U -irreducible part $\varphi^{U\text{irr}}$ [analogous to Eq. (63)] and the bare vertex U [Eq. (64)]. It remains to show that for the U - r -reducible terms $\nabla_r = \bar{\lambda}_r \cdot w_r \cdot \lambda_r$, the components ∇_r^α have the form given in Fig. 1 of Ref. [15], with $\alpha = \text{ch}$ or sp .

We start with the t channel. Defining sign factors for charge and spin channels, $s^{\text{ch}} = 1$ and $s^{\text{sp}} = -1$, we have

$$\begin{aligned}\nabla_t^\alpha &= \nabla_t^{\uparrow\uparrow} + s^\alpha \nabla_t^{\uparrow\downarrow} \\ &= \bar{\lambda}_t^{\uparrow\uparrow|\sigma\uparrow} w_t^{\sigma'\sigma|\sigma'\sigma} \lambda_t^{\uparrow\sigma'|\uparrow\sigma'} + s^\alpha \bar{\lambda}_t^{\sigma\downarrow|\sigma\downarrow} w_t^{\sigma'\sigma|\sigma'\sigma} \lambda_t^{\uparrow\sigma'|\uparrow\sigma'}.\end{aligned}\quad (65)$$

Here, we sum as usual over spin indices σ, σ' . Making use of $w_t^{\uparrow\uparrow} = w_t^{\downarrow\downarrow}$, $w_t^{\downarrow\uparrow} = w_t^{\uparrow\downarrow}$, and similarly for $\bar{\lambda}_t, \lambda_t$, we can collect the summands as

$$\begin{aligned}\nabla_t^\alpha &= (\bar{\lambda}_t^{\uparrow\uparrow} + s^\alpha \bar{\lambda}_t^{\downarrow\downarrow})(w_t^{\uparrow\uparrow} + s^\alpha w_t^{\downarrow\downarrow})(\lambda_t^{\uparrow\uparrow} + s^\alpha \lambda_t^{\downarrow\downarrow}) \\ &= \bar{\lambda}_t^\alpha w_t^\alpha \lambda_t^\alpha,\end{aligned}\quad (66)$$

which is equivalent to ∇^{ph} in Ref. [15]. (Note that in our convention of depicting diagrams, all diagrams are mirrored along the diagonal from the top left to bottom right (i.e., the bottom left and top right legs are exchanged) compared to the convention used in Ref. [15]: The ph ($\bar{\text{ph}}$) channel corresponds to the t (a) channel.)

We continue with the a channel, which is related to the t channel by crossing symmetry,

$$\hat{\Gamma}^{\uparrow\downarrow}(\omega_a, \nu_a, \nu'_a) = -\Gamma^{\uparrow\downarrow}(\omega_t = \omega_a, \nu_t = \nu_a, \nu'_t = \nu'_a). \quad (67)$$

The frequency arguments on the right are defined according to the t -channel conventions $(\omega_t, \nu_t, \nu'_t)$, and then evaluated at the a -channel frequencies occurring on the left. In particular, we have (cf. Eq. (11) of Ref. [15])

$$\begin{aligned}\Gamma^\alpha(\omega_a, \nu_a, \nu'_a) \\ = -\frac{1}{2} [\Gamma^{\text{ch}} + (1 + 2s^\alpha)\Gamma^{\text{sp}}] (\omega_t = \omega_a, \nu_t = \nu_a, \nu'_t = \nu'_a).\end{aligned}\quad (68)$$

The U - a -reducible diagrams ∇_a can therefore be expressed through the U - t -reducible diagrams ∇_t :

$$\begin{aligned}\nabla_a^\alpha(\omega_a, \nu_a, \nu'_a) \\ = -\frac{1}{2} [\bar{\lambda}_t^{\text{ch}} w_t^{\text{ch}} \lambda_t^{\text{ch}} + (1 + 2s^\alpha) \bar{\lambda}_t^{\text{sp}} w_t^{\text{sp}} \lambda_t^{\text{sp}}] (\omega_a, \nu_a, \nu'_a),\end{aligned}\quad (69)$$

reproducing $\nabla^{\bar{\text{ph}}}$ in Ref. [15]. The frequency arguments on the right have the same meaning as in Eq. (67).

Last, we consider the p channel. With SU(2) symmetry, $\nabla_p^{\uparrow\uparrow} = \nabla_p^{\downarrow\downarrow} + \hat{\nabla}_p^{\uparrow\downarrow}$, we have

$$\begin{aligned}\nabla_p^\alpha &= \nabla_p^{\uparrow\uparrow} + s^\alpha \nabla_p^{\downarrow\downarrow} = \hat{\nabla}_p^{\uparrow\downarrow} + (1 + s^\alpha) \nabla_p^{\uparrow\downarrow} \\ &= \bar{\lambda}_p^{\uparrow\downarrow|\sigma\bar{\sigma}} w_p^{\sigma\bar{\sigma}|\sigma'\bar{\sigma}'} \lambda_p^{\sigma'\bar{\sigma}'|\uparrow\downarrow} \\ &\quad + (1 + s^\alpha) \bar{\lambda}_p^{\uparrow\downarrow|\sigma\bar{\sigma}} w_p^{\sigma\bar{\sigma}|\sigma'\bar{\sigma}'} \lambda_p^{\sigma'\bar{\sigma}'|\downarrow\uparrow}.\end{aligned}\quad (70)$$

Note that the spins in the first and second pair of spin indices of w_p have to be opposite, $\sigma\bar{\sigma}$ and $\sigma'\bar{\sigma}'$, since they connect to the same bare vertex (cf. Fig. 11), and $U^{\sigma\sigma} = 0$. Furthermore, the crossing relation $U^{\uparrow\downarrow} = -\hat{U}^{\uparrow\downarrow}$ implies $w_p^{\uparrow\downarrow} = -\hat{w}_p^{\uparrow\downarrow}$. By use of this, we can combine the terms in the spin sums as

$$\begin{aligned}\nabla_p^\alpha &= \frac{s^\alpha}{2} (\bar{\lambda}_p^{\uparrow\downarrow} - \hat{\lambda}_p^{\uparrow\downarrow})(w_p^{\uparrow\downarrow} - \hat{w}_p^{\uparrow\downarrow})(\lambda_p^{\uparrow\downarrow} - \hat{\lambda}_p^{\uparrow\downarrow}) \\ &= \frac{s^\alpha}{2} \bar{\lambda}_p^{\text{si}} w_p^{\text{si}} \lambda_p^{\text{si}},\end{aligned}\quad (71)$$

which gives ∇^{pp} in Ref. [15].

In summary, we thus reproduce the decomposition of Ref. [15]:

$$\Gamma^\alpha = \varphi^{U_{\text{irr},\alpha}} + \nabla_a^\alpha + \nabla_p^\alpha + \nabla_t^\alpha - 2U^\alpha, \quad (72a)$$

where the the U - r -reducible parts are defined as

$$\begin{aligned}\nabla_a^\alpha(\omega_a, \nu_a, \nu'_a) &= -\frac{1}{2} \nabla_t^{\text{ch}}(\omega_a, \nu_a, \nu'_a) \\ &\quad - \left(\frac{3}{2} - 2\delta_{\alpha,\text{sp}}\right) \nabla_t^{\text{sp}}(\omega_a, \nu_a, \nu'_a),\end{aligned}\quad (72b)$$

$$\nabla_p^\alpha(\omega_p, \nu_p, \nu'_p) = \left(\frac{1}{2} - \delta_{\alpha,\text{sp}}\right) [\bar{\lambda}_p^{\text{si}} w_p^{\text{si}} \lambda_p^{\text{si}}](\omega_p, \nu_p, \nu'_p), \quad (72c)$$

$$\nabla_t^\alpha(\omega_t, \nu_t, \nu'_t) = [\bar{\lambda}_t^\alpha w_t^\alpha \lambda_t^\alpha](\omega_t, \nu_t, \nu'_t). \quad (72d)$$

E Alternative derivation of SBE mfRG flow

In the main text, we derived the SBE multiloop flow equations by inserting the SBE decomposition into the known multiloop flow equations of the two-particle reducible vertices γ_r . They can also be derived without prior knowledge on the flow of γ_r , by using the techniques of Ref. [7].

In the parquet setting of Ref. [7], one can view the Π - r -irreducible vertex I_r as the key ingredient for all equations related to channel r . In step (i), one uses I_r to generate γ_r and thus Γ through a BSE. Then, a post-processing of attaching and closing external legs yields (ii) a three-point vertex $\Gamma_r^{(3)}$ and (iii) a susceptibility χ_r . The SBE setting of the main text can be understood in close analogy, with the only exception that one purposefully avoids to generate U - r -reducible contributions, because these can (more efficiently) be constructed via $\nabla_r = \bar{\lambda}_r \cdot w_r \cdot \lambda_r$. To exclude U - r -reducible contributions, one uses in step (i) $I_r - U$ to generate M_r and thus T_r through a BSE. The same post-processing as before yields (ii) λ_r and then (iii) w_r (through the polarization, see below).

Because of this analogy, the SBE multiloop flow equations can be derived in the exact same fashion as the multiloop flow equations of Ref. [7]. One merely has to replace the variables $I_r \rightarrow I_r - U$, $\Gamma \rightarrow T_r$, $\gamma_r \rightarrow M_r$, $\Gamma_r^{(3)} \rightarrow \lambda_r$, $\chi_r \rightarrow P_r$. P_r is the polarization [21]

$$P_r(\omega_r) = \sum_{\nu_r''} \Pi_r(\omega_r, \nu_r'') \cdot \bar{\lambda}_r(\omega_r, \nu_r''), \quad (73)$$

which allows one to express the screened interaction through a Dyson equation as

$$w_r = U + U \cdot P_r \cdot w_r \Leftrightarrow w_r = (\mathbf{1}_r - U \cdot P_r)^{-1} \cdot U. \quad (74)$$

For step (i), the analogous two sets of equations are

$$\Gamma = I_r + \gamma_r, \quad \gamma_r = I_r \circ \Pi_r \circ \Gamma, \quad (75a)$$

$$T_r = (I_r - U) + M_r, \quad M_r = (I_r - U) \circ \Pi_r \circ T_r. \quad (75b)$$

They yield flow equations of identical structure, after replacing the variables as stated above:

$$\dot{\gamma}_r = f_1[\Gamma, \Pi_r, \dot{\Pi}_r, \dot{I}_r], \quad (76a)$$

$$\dot{M}_r = f_1[T_r, \Pi_r, \dot{\Pi}_r, \dot{I}_r]. \quad (76b)$$

For the last argument of Eq. (76b), we used $\partial_\Lambda(I_r - U) = \dot{I}_r$, as $\dot{U} = 0$. The functional f_1 is

$$f_1[T_r, \Pi_r, \dot{\Pi}_r, \dot{I}_r] = T_r \circ \dot{\Pi}_r \circ T_r + \dot{I}_r \circ \Pi_r \circ T_r + T_r \circ \Pi_r \circ \dot{I}_r \circ \Pi_r \circ T_r + T_r \circ \Pi_r \circ \dot{I}_r, \quad (76c)$$

cf. Eq. (10) and Fig. 2(a) of Ref. [7]. A loop expansion with $\dot{I}_r = \sum_\ell \dot{\gamma}_r^{(\ell)}$ then yields Eqs. (48) and Fig. 9.

In step (ii), we have the two analogous relations

$$\Gamma_r^{(3)} = \mathbf{1}_r + \sum_{\nu''} \Pi_r \bullet \Gamma, \quad \lambda_r = \mathbf{1}_r + \sum_{\nu''} \Pi_r \bullet T_r. \quad (77a)$$

They again yield flow equations of identical structure after replacing variables:

$$\dot{\Gamma}_r^{(3)} = f_2[\Gamma_r^{(3)}, \Gamma, \Pi_r, \dot{\Pi}_r, \dot{I}_r], \quad (78a)$$

$$\dot{\lambda}_r = f_2[\lambda_r, T_r, \Pi_r, \dot{\Pi}_r, \dot{I}_r]. \quad (78b)$$

The functional f_2 is given by

$$f_2[\lambda_r, T_r, \Pi_r, \dot{\Pi}_r, \dot{I}_r] = \lambda_r \circ \dot{\Pi}_r \circ T_r + \lambda_r \circ \Pi_r \circ (\dot{I}_r + \dot{I}_r \circ \Pi_r \circ T_r), \quad (78c)$$

cf. Eqs. (42) (with $\Gamma_{r,0}^{(3)} = \mathbf{1}_r$) and Fig. 7 of Ref. [7]. A loop expansion again gives our Eqs. (48) and Fig. 9.

Finally, in step (iii), the susceptibility and polarization obey the two relations

$$\chi_r = \sum_{\nu''} \Pi_r \bullet \bar{\Gamma}_r^{(3)}, \quad P_r = \sum_{\nu''} \Pi_r \bullet \bar{\lambda}_r. \quad (79a)$$

Hence, we get perfectly analogous flow equations

$$\dot{\chi}_r = f_3[\Gamma_r^{(3)}, \Pi_r, \dot{\Pi}_r, \dot{I}_r], \quad (80a)$$

$$\dot{P}_r = f_3[\lambda_r, \Pi_r, \dot{\Pi}_r, \dot{I}_r], \quad (80b)$$

$$f_3[\lambda_r, \Pi_r, \dot{\Pi}_r, \dot{I}_r] = \lambda_r \circ \dot{\Pi}_r \circ \bar{\lambda}_r + \lambda_r \circ \Pi_r \circ \dot{I}_r \circ \Pi_r \circ \bar{\lambda}_r, \quad (80c)$$

cf. Eq. (44) and Fig. 8 of Ref. [7]. Finally, Eq. (74) yields

$$\dot{w}_r = U \bullet \dot{P}_r \bullet w_r + U \bullet P_r \bullet \dot{w}_r. \quad (81a)$$

Solving this for \dot{w}_r , we obtain

$$\dot{w}_r = (\mathbf{1}_r - U \bullet P_r)^{-1} \bullet U \bullet \dot{P}_r \bullet w_r = w_r \bullet \dot{P}_r \bullet w_r. \quad (81b)$$

Again, a loop expansion yields the same flow equation for w_r as in our Eqs. (48) and Fig. 9.

References

1. T. Schäfer, N. Wentzell, F. Šimkovic, Y.Y. He, C. Hille, M. Klett, C.J. Eckhardt, B. Arzhang, V. Harkov, F.M. Le Régent et al., Phys. Rev. X **11**, 011058 (2021)
2. W. Metzner, M. Salmhofer, C. Honerkamp, V. Meden, K. Schönhammer, Rev. Mod. Phys. **84**, 299 (2012)
3. P. Kopietz, L. Bartosch, F. Schütz, *Introduction to the functional renormalization group*, Vol. 798 (Springer, 2010)
4. J. Diekmann, S.G. Jakobs, Phys. Rev. B **103**, 155156 (2021)
5. F.B. Kugler, J. von Delft, Phys. Rev. B **97** (2018)
6. F.B. Kugler, J. von Delft, Phys. Rev. Lett. **120** (2018)
7. F.B. Kugler, J. von Delft, New J. Phys. **20**, 123029 (2018)
8. B. Roulet, J. Gavoret, P. Nozières, Phys. Rev. **178**, 1072 (1969)
9. N.E. Bickers, in *in: Sénéchal D., Tremblay A.-M., Bourbonnais C. (eds), Theoretical Methods for Strongly Correlated Electrons, CRM Series in Mathematical Physics* (Springer, New York, 2004)
10. G. Li, N. Wentzell, P. Pudleiner, P. Thunström, K. Held, Phys. Rev. B **93**, 165103 (2016)
11. N. Wentzell, G. Li, A. Tagliavini, C. Taranto, G. Rohringer, K. Held, A. Toschi, S. Andergassen, Phys. Rev. B **102**, 085106 (2020)
12. C. Husemann, M. Salmhofer, Phys. Rev. B **79**, 195125 (2009)
13. C. Husemann, K.U. Giering, M. Salmhofer, Phys. Rev. B **85**, 075121 (2012)
14. E.G.C.P. van Loon, F. Krien, H. Hafermann, A.I. Lichtenstein, M.I. Katsnelson, Phys. Rev. B **98**, 205148 (2018)
15. F. Krien, A. Valli, M. Capone, Phys. Rev. B **100**, 155149 (2019)
16. F. Krien, Phys. Rev. B **99**, 235106 (2019)
17. F. Krien, A. Valli, Phys. Rev. B **100**, 245147 (2019)
18. V. Harkov, A.I. Lichtenstein, F. Krien, Phys. Rev. B **104**, 125141 (2021)
19. F. Krien, A.I. Lichtenstein, G. Rohringer, Phys. Rev. B **102**, 235133 (2020)
20. F. Krien, A. Valli, P. Chalupa, M. Capone, A.I. Lichtenstein, A. Toschi, Phys. Rev. B **102**, 195131 (2020)
21. F. Krien, A. Kauch, K. Held, Phys. Rev. Research **3**, 013149 (2021)
22. P.M. Bonetti, A. Toschi, C. Hille, S. Andergassen, D. Vilardi, arXiv:2105.11749 [cond-mat.str-el] (2021), 2105.11749
23. C. Taranto, S. Andergassen, J. Bauer, K. Held, A. Katanin, W. Metzner, G. Rohringer, A. Toschi, Phys. Rev. Lett. **112**, 196402 (2014)
24. D. Vilardi, C. Taranto, W. Metzner, Phys. Rev. B **99**, 104501 (2019)
25. A.A. Katanin, Phys. Rev. B **99**, 115112 (2019)
26. A. Altland, B.D. Simons, *Condensed matter field theory* (Cambridge University Press, 2010)
27. A. Kamenev, *Field theory of non-equilibrium systems* (Cambridge University Press, 2011)
28. G. Rohringer, A. Valli, A. Toschi, Phys. Rev. B **86**, 125114 (2012)
29. A.A. Katanin, Phys. Rev. B **70**, 115109 (2004)
30. T. Schäfer, G. Rohringer, O. Gunnarsson, S. Ciuchi, G. Sangiovanni, A. Toschi, Phys. Rev. Lett. **110**, 246405 (2013)
31. T. Schäfer, S. Ciuchi, M. Wallerberger, P. Thunström, O. Gunnarsson, G. Sangiovanni, G. Rohringer, A. Toschi, Phys. Rev. B **94**, 235108 (2016)
32. O. Gunnarsson, G. Rohringer, T. Schäfer, G. Sangiovanni, A. Toschi, Phys. Rev. Lett. **119**, 056402 (2017)
33. P. Chalupa, P. Gunacker, T. Schäfer, K. Held, A. Toschi, Phys. Rev. B **97**, 245136 (2018)

34. P. Thunström, O. Gunnarsson, S. Ciuchi, G. Rohringer, *Phys. Rev. B* **98**, 235107 (2018)
35. F.B. Kugler, S.S.B. Lee, J. von Delft, *Phys. Rev. X* **11**, 041006 (2021)
36. S.S.B. Lee, F.B. Kugler, J. von Delft, *Phys. Rev. X* **11**, 041007 (2021)
37. E. Walter, Ph.D. thesis, Ludwig-Maximilians-Universität München (2021)
38. S. Aguirre Lamus, Master's thesis, Ludwig-Maximilians-Universität München (2020)
39. G. Rohringer, Ph.D. thesis, TU Wien (2013)